

LONGITUDINAL EFFECTS AND FOCUSING IN
SPACE-CHARGE DOMINATED BEAMS

by

John Richardson Harris

Thesis submitted to the Faculty of the Graduate School of the
University of Maryland, College Park in partial fulfillment
of the requirements for the degree of
Master of Science
2002

Advisory Committee:

Professor Patrick G. O'Shea, Chair
Professor Victor L. Granatstein
Professor Martin Reiser

ABSTRACT

Title of Thesis: LONGITUDINAL EFFECTS AND FOCUSING IN
SPACE-CHARGE DOMINATED BEAMS

Degree candidate: John Richardson Harris

Degree and year: Master of Science, 2002

Thesis directed by: Professor Patrick G. O'Shea

Department of Electrical and Computer Engineering

The purpose of this thesis is to investigate longitudinal effects in space-charge dominated beams, and to begin design of a longitudinal focusing system for the University of Maryland Electron Ring (UMER). The longitudinal envelope equation is introduced and used to develop a longitudinal intensity parameter which is analogous to the transverse intensity parameter. After solving for the free-expansion longitudinal envelope, the electric field necessary to properly focus a parabolic beam in a periodic longitudinal focusing lattice is determined. The cold fluid model for space-charge dominated beams is then introduced, and results stated for the free expansion of a rectangular beam pulse. A more general approach to find the electric field needed in a periodic longitudinal focusing lattice is then developed. This approach is applicable, within certain assumptions, to any beam profile for which the particle velocity and line charge density can be determined through theory or simulation. The drift compression focusing scheme discussed heavily in the literature is explored and problems with this method are noted. Some discrepancies and areas where further work is needed are also addressed.

PREFACE

The original version of this thesis was submitted to the University of Maryland in printed form in 2002. This version was assembled from the original source files, but may contain minor differences as compared to the official version on file with the University.

J.R. Harris
May 27, 2006

ACKNOWLEDGEMENTS

I would like to thank my committee for making this thesis and defense possible. In addition, I would like to thank Professor Patrick O'Shea and Professor Martin Reiser for their guidance during the past year, Dr. Agust Valfells for valuable discussions on theory, and Dr. Irving Haber and Dr. Rami Kishek for assistance with simulations.

TABLE OF CONTENTS

List of Tables	v
List of Figures	vi
1. Introduction	1
2. Longitudinal Envelope Equation.	6
2.1. Introduction.	6
2.2. Longitudinal Intensity Parameter.	8
2.3. Solutions of the Longitudinal Envelope Equation.	14
2.4. Longitudinal Focusing for Parabolic Beams.	21
2.5. Limitations	28
3. One-Dimensional Cold Fluid Model.	30
3.1. Introduction.	30
3.2. Governing Equations.	30
3.3. Rectangular Beam Expansion and the Method of Characteristics.	32
3.4. Coherent Energy Spread.	36
3.5. Discrepancies.	38
4. Longitudinal Focusing in UMER: A more general approach.	42
4.1. Introduction.	42
4.2. Longitudinal Focusing.	42
4.3. Drift Compression.	47
5. Additional Effects.	51
6. Longitudinal Experiments.	54

6.1. Introduction.	54
6.2. UMER Facility and Diagnostics.	54
6.3. Longitudinal Experiments not requiring Induction Gaps.	55
6.4. Longitudinal Experiments requiring Induction Gaps.	58
7. Conclusion.	62
References.	64

LIST OF TABLES

1.	Longitudinal Intensity Parameter for UMER.	11
2.	Comparison of Longitudinal and Transverse Relations.	17

LIST OF FIGURES

1.	Space Charge Intensity Parameter (χ).	3
2.	University of Maryland Electron Ring (UMER).	4
3.	Longitudinal Space Charge Intensity Parameter (χ_L).	16
4.	Longitudinal Envelope for a Contracting Beam.	20
5.	Beam Undergoing Contraction and Formation Simultaneously.	20
6.	Expansion of Parabolic Beam in UMER.	22
7.	Longitudinal Focusing Lattice.	23
8.	Electric Field for Focusing Parabolic Bunch.	29
9.	Fluid Analogy for Expansion of Rectangular Electron Beam.	35
10.	Line Charge Density and Velocity in Expanding Rectangular Beam.	36
11.	Conceptual Layout of Induction Gap in the Rest Frame of the Beam.	44
12.	Longitudinal Focusing Voltages for Rectangular Beam.	49

1. Introduction.

The behavior of charged particle beams and the focusing methods needed to control them depend in part on beam intensity. Low intensity beams are characterized by low space-charge density, and their response to external focusing is governed primarily by thermal effects (emittance). The transport of emittance dominated beams in focusing systems is similar to the transport of light through an optical focusing system. High intensity beams are characterized by high space-charge density, and the electric forces between the particles in the beam govern its behavior in focusing systems. Space-charge dominated beams behave like a plasma, with pronounced collective and nonlinear effects.

The intensity parameter (χ) has been introduced to provide a measure of beam intensity[1]. This parameter is the ratio of the transverse space-charge force to the transverse focusing force in a beam, and is given by

$$\chi = \frac{K}{k_0^2 R^2}, \quad (1)$$

where K is the generalized perveance of the beam, k_0 is the betatron oscillation wave number in the absence of space charge, and R is the transverse beam envelope. The generalized perveance is directly related to the space-charge density in the beam. The value of χ ranges from zero (emittance dominated) to one (space-charge dominated); it cannot exceed one, as the space-charge forces would exceed the focusing forces and the beam would no longer be confined by the focusing system.

Although most research has been done on emittance dominated beams, many current and planned applications require space-charge dominated beams. These

applications include high power microwave sources, free-electron lasers, and heavy-ion inertial confinement fusion drivers (HIF)[2-5].

The University of Maryland Electron Ring (UMER), a space-charge dominated beam transport system, is currently under construction, and will be used to improve the understanding of space-charge dominated beams. Although the UMER beam is composed of electrons, it has been designed so that it will behave in a similar manner as the beams of heavy ions such as bismuth that will be needed for planned HIF machines[6]. As such, UMER is a scale model which allows research to be done in support of the HIF program in a university laboratory setting at considerably less expense than would be involved with the actual construction of a HIF driver. A second, related goal for UMER is the investigation of space-charge wave propagation along the direction of travel of intense beams. These longitudinal waves were first studied by D.X. Wang at Maryland in the early 1990's, but this research was limited by the length of the beamline available at the time[7]. Because UMER is a circular machine, the distance over which the beam can propagate is not limited by its physical size. This will allow longitudinal waves to be studied for longer periods of time than were possible in previous machines. UMER also has improved diagnostics which will allow these waves to be studied in more detail than was possible in the past[8-10].

Although UMER is designed to access the very intense region that will be needed for HIF drivers, it can also be tuned across a wide range of χ . This allows it to access the emittance dominated region and the crossover region near $\chi = 0.5$, where both emittance and space charge must be considered.

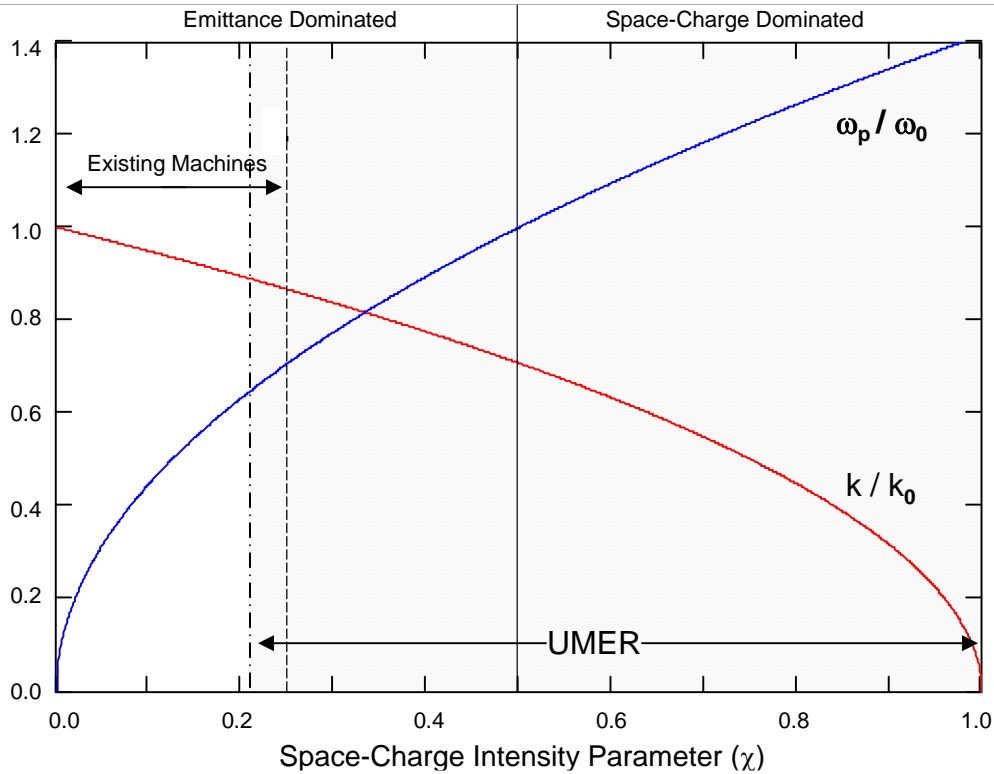


Fig. 1. Space Charge Intensity Parameter (χ). This graph relates the intensity parameter for transverse beam physics with the tune depression (k/k_0) and the plasma frequency (ω_p). Beams with $0 \leq \chi < 0.5$ are considered emittance dominated, while beams with $0.5 < \chi \leq 1$ are considered space charge dominated. Existing rings are emittance dominated, and operate in the range to the left of the dashed line. UMER is designed to operate across a wide range of intensity parameter values, from approximately $\chi = 0.2$ to almost $\chi = 1$. The intended operating range for UMER extends to the right of the dash-dot line.

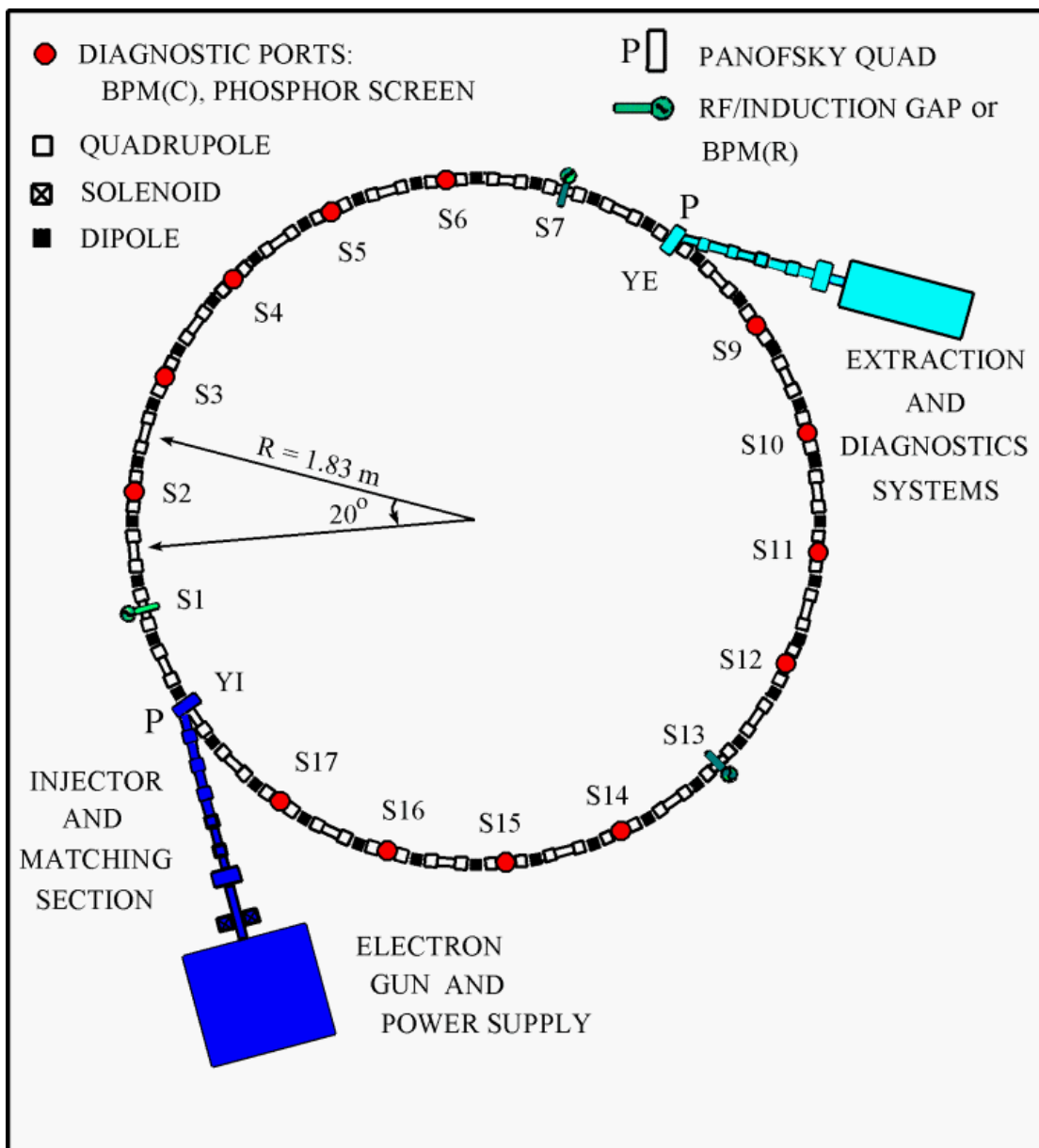


Fig. 2. The University of Maryland Electron Ring (UMER)[11].

Most of the work done on focusing in UMER has been concentrated on its transverse focusing system. However, space charge will also drive an expansion of the beam along its axis of travel. In order to control this longitudinal expansion, a longitudinal focusing system must be implemented. This system will use induction gaps to apply an electric field to the beam along its direction of travel, which will compress the beam longitudinally.

The purpose of this thesis is to investigate longitudinal effects in space-charge dominated beams, and to begin design of a longitudinal focusing system for UMER. The longitudinal envelope equation will be introduced and used to develop a longitudinal intensity parameter which is the longitudinal analog to the intensity parameter of eq. (1). After solving for the free-expansion longitudinal envelope, the electric field necessary to properly focus a parabolic beam in a periodic longitudinal focusing lattice will be determined. The cold fluid model for space-charge dominated beams will then be introduced, and results stated for the free expansion of a rectangular beam pulse. A more general approach to find the electric field needed in a periodic longitudinal focusing lattice will then be developed. This approach is applicable, within certain assumptions, to any beam profile for which the particle velocity and line charge density can be determined through theory or simulation. The drift compression focusing scheme discussed heavily in the literature will be explored and problems with this method will be noted. Some discrepancies and areas where further work is needed will also be addressed.

2. Longitudinal Envelope Equation.

2.1. Introduction.

One approach to investigating longitudinal effects in charged-particle beams is through the longitudinal envelope equation[12]

$$\tilde{z}'' + \kappa_{z0}\tilde{z} - \frac{K_L}{5\sqrt{5}\tilde{z}^2} - \frac{\tilde{\varepsilon}_{zz'}^2}{\tilde{z}^3} = 0, \quad (2)$$

where \tilde{z} is the RMS half length of the beam, κ_{z0} is the longitudinal focusing function,

K_L is the longitudinal generalized perveance, and $\tilde{\varepsilon}_{zz'}$ is the unnormalized RMS

longitudinal emittance. The generalized longitudinal perveance is given by

$$K_L = \frac{3}{2} \frac{gN}{\beta^2 \gamma^5} \frac{q^2}{4\pi\varepsilon_0 mc^2} \quad (3)$$

where N is the total number of particles in the bunch, q is the charge of the electron, ε_0 is the permittivity of free space, m is the mass of the electron, c is the speed of light, and β and γ are the relativistic factors. The focusing function κ_{z0} can be related to the applied electric field, and may be a function of location and time. The unnormalized RMS emittance is given by

$$\tilde{\varepsilon}_{zz'} = \left[\langle z^2 \rangle \langle z'^2 \rangle - \langle zz' \rangle^2 \right]^{1/2}. \quad (4)$$

The geometry factor g is given approximately by $g \approx 1 + 2 \ln\left(\frac{b}{a}\right)$, where b is the radius

of the beam pipe and a is the radius of the beam[7,12]. Note that both the RMS half-

length \tilde{z} and the true half-length z_m are measured from the centroid of the beam in the

beam rest frame. The distance traveled by the beam centroid through the laboratory

frame is denoted s , and primed quantities indicate a derivative with respect to s .

Although β and γ appear throughout this thesis, UMER is strictly nonrelativistic, with a maximum β of 0.2. The presence of β or γ in an equation should not be taken to imply that the equation is correct for relativistic beams.

The longitudinal envelope equation was first derived by L. Smith[13], with additional work being done by Neuffer[14] and Sacherer[15]. Their derivations of the equation were directly applicable only to beams with uniform, parabolic, or Gaussian distributions. Although the beams of interest to UMER are generally not uniform, parabolic, or Gaussian, the parabolic beam can be taken as an equivalent line charge density for a beam with the same number of particles, the same emittance, and the same RMS length[16].

Although the longitudinal envelope equation serves the same role in longitudinal dynamics that the transverse envelope equation serves in transverse dynamics, certain differences should be noted:

1. The longitudinal perveance is not dimensionless as in the transverse case, but rather has dimensions of meters. This is also reflected in the extra factor of length in the denominator of the space-charge term in the longitudinal envelope equation as compared to the transverse envelope equation.
2. The relations between RMS and non-RMS quantities are different. For the longitudinal envelope equation $z_m = \sqrt{5}\tilde{z}$ and $\mathcal{E}_{zz'} = 5\tilde{\mathcal{E}}_{zz'}$, while for the transverse envelope equation $x_m = 2\tilde{x}$ and $\mathcal{E}_x = 4\tilde{\mathcal{E}}$.

3. The angle referred to by the longitudinal emittance does not exist in real space, since \bar{z}' is parallel to the local direction of travel \bar{s} . For transverse emittance, the angle does exist in real space since \bar{x}' is perpendicular to the direction of travel of the beam.

2.2. Longitudinal Intensity Parameter.

Before actually solving the longitudinal envelope equation for specific cases, it is instructive to look in more detail at this equation. The first term, \tilde{z}'' , gives the "acceleration" of the beam edge. Driving this acceleration are three terms: $\kappa_{z0}\tilde{z}$ is a focusing term, which tends to make \tilde{z}'' increasingly negative, resulting in a beam contraction; and $\frac{K_L}{5\sqrt{5}\tilde{z}^2}$ and $\frac{\tilde{\varepsilon}_{zz'}^2}{\tilde{z}^3}$, which due to their signs tend to make \tilde{z}'' positive, driving the beam expansion. For beams which are strongly space-charge dominated, the emittance term can be neglected, while for beams which are strongly emittance dominated, the space-charge (perveance) term can be neglected. In order to determine whether the beam is space-charge dominated or emittance dominated, a longitudinal intensity parameter can be introduced. This parameter is the longitudinal analog to χ . For consistency with the transverse case the non-RMS longitudinal envelope equation[12] is used:

$$z_m'' + \kappa_{z0}z_m - \frac{K_L}{z_m^2} - \frac{\varepsilon_{zz'}^2}{z_m^3} = 0. \quad (5)$$

This non-RMS equation describes the envelope of the extreme edge (half-length) of the beam, z_m , and can be derived from the RMS equation by use of the relations between RMS and non-RMS quantities. Since the transverse intensity parameter is the ratio

between the space-charge force and the focusing force for a matched beam, we take

$z_m'' = 0$ to obtain the longitudinal matched beam envelope equation:

$$k_{0L}^2 z_m - \frac{K_L}{z_m^2} - \frac{\varepsilon_{zz'}^2}{z_m^3} = 0. \quad (6)$$

Here, the focusing function κ_{z0} has been replaced by the zero-current synchrotron wave number k_{0L}^2 to indicate that focusing is continuous for a matched beam. In general, the focusing function κ_{z0} varies throughout the focusing system. Then by analogy with χ , we take

$$\chi_L = \frac{\text{longitudinal space - charge force}}{\text{longitudinal focusing}}$$

$$\chi_L = \frac{K_L}{k_{0L}^2 z_m^3}. \quad (7)$$

Since the goal is to obtain a single number to describe the overall behavior of the beam, uniform focusing is assumed and χ_L is rewritten in terms of generalized longitudinal perveance, beam half-length, and longitudinal emittance, using eq. (6).

$$\chi_L = \frac{K_L}{\left(\frac{K_L}{z_m^2} + \frac{\varepsilon_{zz'}^2}{z_m^3} \right) z_m^2}$$

$$\chi_L = \frac{K_L}{K_L + \frac{\varepsilon_{zz'}^2}{z_m}}. \quad (8)$$

Longitudinal emittance (unnormalized effective emittance) can be rewritten in terms of longitudinal energy spread, which can be measured[9,12,17].:

$$\varepsilon_{zz'} = 5\tilde{\varepsilon}_{zz'}$$

$$\begin{aligned}
\varepsilon_{zz'} &= 5 \frac{\tilde{\varepsilon}_{nz}}{\beta\gamma^3} \\
\varepsilon_{zz'} &= \frac{5}{\beta\gamma^3} \tilde{z} \left(\frac{\gamma^3 k_B T_{\parallel}}{mc^2} \right)^{1/2} \\
\varepsilon_{zz'} &= \frac{5}{\beta\gamma^3} \tilde{z} \left(\frac{\gamma}{\beta E c} \Delta \tilde{E} \right) \\
\varepsilon_{zz'} &= \frac{5}{\beta\gamma^3} \frac{z_m}{\sqrt{5}} \left(\frac{\Delta \tilde{E}}{\gamma mc^2} \frac{\gamma}{\beta} \right) \\
\varepsilon_{zz'} &= \frac{5}{\beta^2 \gamma^3} \frac{z_m}{\sqrt{5}} \frac{\Delta \tilde{E}}{mc^2}. \tag{9}
\end{aligned}$$

Using this result in eq. (8) gives

$$\chi_L = \frac{K_L}{K_L + \left[\frac{\sqrt{5}}{\beta^2 \gamma^3} \frac{\Delta \tilde{E}}{mc^2} \right]^2 z_m}. \tag{10}$$

Table 1 shows that, while UMER's transverse intensity χ can be adjusted across a wide range of values, from space-charge dominated to emittance dominated, the longitudinal behavior of UMER will always be space-charge dominated for practical operating parameters.

The transverse intensity parameter is particularly useful because it can be related to other parameters used in beam and plasma physics through simple expressions. This is also true for the longitudinal intensity parameter χ_L as derived above. For example, χ_L has the same relationship to the longitudinal tune depression that the transverse intensity

	Case 1	Case2	Case3	Case4	Case5
Current	100 mA	100 mA	1 mA	1 mA	1 mA
Pulse Length	100 ns	70 ns	70 ns	70 ns	70 ns
Energy Spread	10 eV	10 eV	10 eV	50 eV	100 eV
χ_L	0.99979	0.99979	0.97957	0.65734	0.3241
$\varepsilon_{zz'}$	0.00345 m	0.00241 m	0.00241 m	0.0121 m	0.0241
T_{\parallel}	53.26 K	53.26 K	53.26 K	1331.6 K	5326.3 K

Table 1. Longitudinal Intensity Parameter for UMER. In Cases 1, 2, and 3, the beam is almost totally space charge dominated. Cases 4 and 5 cannot be realized with UMER, but were included to show examples of operating parameters which would result in a longitudinal intensity different from $\chi_L \approx 1$. Note that the perpendicular temperature T_{\perp} is 1453.7 K, which shows that the beam will not normally be in thermal equilibrium between its transverse and longitudinal properties. Thermal equilibrium is approximately achieved in Case 4. Operating parameters assumed for UMER were: $\beta = 0.2$, beam radius 1 cm, transverse normalized effective emittance 10 μm .

parameter χ has to the transverse tune depression, namely

$$\frac{k_L}{k_{0L}} = \sqrt{1 - \chi_L} \quad (11)$$

in the longitudinal case. The synchrotron wave number with space charge (k_L) and the synchrotron wave number without space charge (k_{0L}) are related by

$$k_L^2 = k_{0L}^2 - \frac{K_L}{z_m^3} \quad (11a)$$

where

$$k_{0L}^2 = \kappa_{z0}.$$

For the transverse case, the betatron wave numbers with and without space charge (k and k_0) are used. Betatron and synchrotron oscillations are analogous, with the former referring to transverse motion while the latter refers to longitudinal motion. Eq. (11a) is derived from the longitudinal envelope equation by following the same procedure used to derive the transverse tune depression from the transverse envelope equation.

A second transverse beam parameter, the plasma frequency ω_p , is related to the transverse intensity parameter through the relation

$$\frac{\omega_p}{\omega_0} = \sqrt{2\chi}. \quad (12)$$

The transverse zero-current betatron frequency $\omega_0 = k_0 v$ relates the zero-current betatron wave number (k_0) to the beam velocity. A longitudinal plasma frequency ω_{pL} can also be defined. A relationship between the longitudinal intensity parameter and the longitudinal plasma frequency can be written which is similar to that between the transverse intensity parameter and the transverse plasma frequency. However, because

the dependence of the space charge term on position is different longitudinally than transversely, the analogous longitudinal equation is slightly different. For transverse motion of a particle in a beam[12],

$$\ddot{x} = \omega_p^2 x = \frac{qE_s}{\gamma^3 m}, \quad (13)$$

where x is the location of the particle, \ddot{x} is the particle's acceleration, and E_s is the electric field due to space charge experienced by the particle. This takes into account relativistic effects which reduce the force between electric charges. For longitudinal motion, postulate

$$\ddot{z} = \omega_{pL}^2 z = \frac{qE_{sz}}{\gamma^3 m}. \quad (14)$$

The longitudinal electric field due to space charge is normally taken as

$$E_{sz} = -\frac{g}{4\pi\epsilon_0\gamma^2} \frac{\partial\lambda}{\partial z}, \quad (15)$$

and for a parabolic beam the line charge density λ is given by[12],

$$\lambda(z) = \lambda_0 \left(1 - \frac{z^2}{z_m^2} \right), \quad (16)$$

where λ_0 is the peak line charge density and z is the location in the beam. Combining eqs. (14), (15), and (16),

$$\ddot{z} = \omega_{pL}^2 z = \frac{gq}{4\pi\epsilon_0\gamma^5 m} \lambda_0 \left(\frac{2z}{z_m^2} \right), \quad (17)$$

so

$$\omega_{pL}^2 = \frac{2gq\lambda_0}{m\gamma^5 4\pi\epsilon_0 z_m^2}. \quad (18)$$

But the average line charge density can be written in terms of the full length (twice the half length) of the beam and the number of particles as $\tilde{\lambda}_0 = \frac{qN}{2z_m}$. The relationship

between the peak line charge density and the RMS average line charge density can be shown to be $\tilde{\lambda}_0 = \frac{4}{\sqrt{30}}\lambda_0$. The plasma frequency can then be rewritten as

$$\omega_{pL}^2 = \left(\frac{3}{2} \frac{gNq^2}{\beta^2 \gamma^5 4\pi\epsilon_0 mc^2} \right) \frac{\sqrt{30}}{6} \frac{v^2}{z_m^3},$$

or

$$\omega_{pL}^2 = \sqrt{\frac{5}{6}} \frac{K_L v^2}{z_m^3}. \quad (19)$$

This is similar to a form of the expression for the transverse plasma frequency

$$\omega_p^2 = \frac{2Kv^2}{r_m^2}, \quad (20)$$

except for the cubed dependence on position (needed because transverse perveance is

dimensionless while longitudinal perveance has units of meters) and the factor of $\sqrt{\frac{5}{6}}$.

The longitudinal version of eq. (12) can be found by dividing eq. (19) by the zero-current synchrotron frequency $\omega_{0L} = k_{0L}v$ and using the definition of χ_L from eq. (7):

$$\frac{\omega_{pL}}{\omega_{0L}} = \sqrt{\sqrt{\frac{5}{6}}\chi_L} \approx \sqrt{0.91\chi_L}. \quad (21)$$

2.3. Solutions of the Longitudinal Envelope Equation.

We now proceed to solve the longitudinal envelope equation for certain cases. An approximate solution to the stationary equation ($z'' = 0$) has been found previously[18] to be

$$z_m \approx \left(\frac{\varepsilon_{zz'}^{3/2}}{k_{0L}^{3/2}} + \frac{K_L}{k_{0L}^2} \right)^{1/3}. \quad (22)$$

However, the design of UMER, with longitudinal focusing applied at only three points, means that the beam will not be stationary.

To solve for the nonstationary case, we first rewrite the longitudinal envelope equation (eq. 2) as

$$\frac{d^2 \tilde{z}}{ds^2} = \frac{K_L}{5\sqrt{5}\tilde{z}^2} + \frac{\tilde{\varepsilon}_{zz'}^2}{\tilde{z}^3} - \kappa_{z0} \tilde{z}, \quad (23)$$

where the derivative has been made explicit. This equation cannot be integrated

immediately. Instead, we multiply both sides by $2 \frac{d\tilde{z}}{ds}$ [19].

$$2 \frac{d\tilde{z}}{ds} \frac{d^2 \tilde{z}}{ds^2} = 2 \frac{d\tilde{z}}{ds} \frac{d}{ds} \frac{d\tilde{z}}{ds} = 2 \frac{d\tilde{z}}{ds} \left(\frac{K_L}{5\sqrt{5}\tilde{z}^2} + \frac{\tilde{\varepsilon}_{zz'}^2}{\tilde{z}^3} - \kappa_{z0} \tilde{z} \right) \quad (24)$$

$$2 \int_{\tilde{z}_0}^{\tilde{z}} \frac{d\tilde{z}}{ds} d \frac{d\tilde{z}}{ds} = 2 \int_{\tilde{z}_0}^{\tilde{z}} \left(\frac{K_L}{5\sqrt{5}\tilde{z}^2} + \frac{\tilde{\varepsilon}_{zz'}^2}{\tilde{z}^3} - \kappa_{z0} \tilde{z} \right) d\tilde{z}$$

$$\left(\frac{d\tilde{z}}{ds} \right)^2 = 2 \left[-\frac{K_L}{5\sqrt{5}} \tilde{z}^{-1} - \frac{\tilde{\varepsilon}_{zz'}^2 \tilde{z}^{-2}}{2} - \frac{\kappa_{z0} \tilde{z}^2}{2} \right]_{\tilde{z}_0}^{\tilde{z}} + \left(\left[\frac{d\tilde{z}}{ds} \right]_{\tilde{z}_0, s_0} \right)^2 \quad (25)$$

In this equation, \tilde{z}_0 is the initial RMS length of the beam, and s_0 is the initial location of the beam center, usually taken as $s_0 = 0$. For space-charge dominated beams with no focusing (free expansion), both the emittance and focusing terms in eq. (25) can be

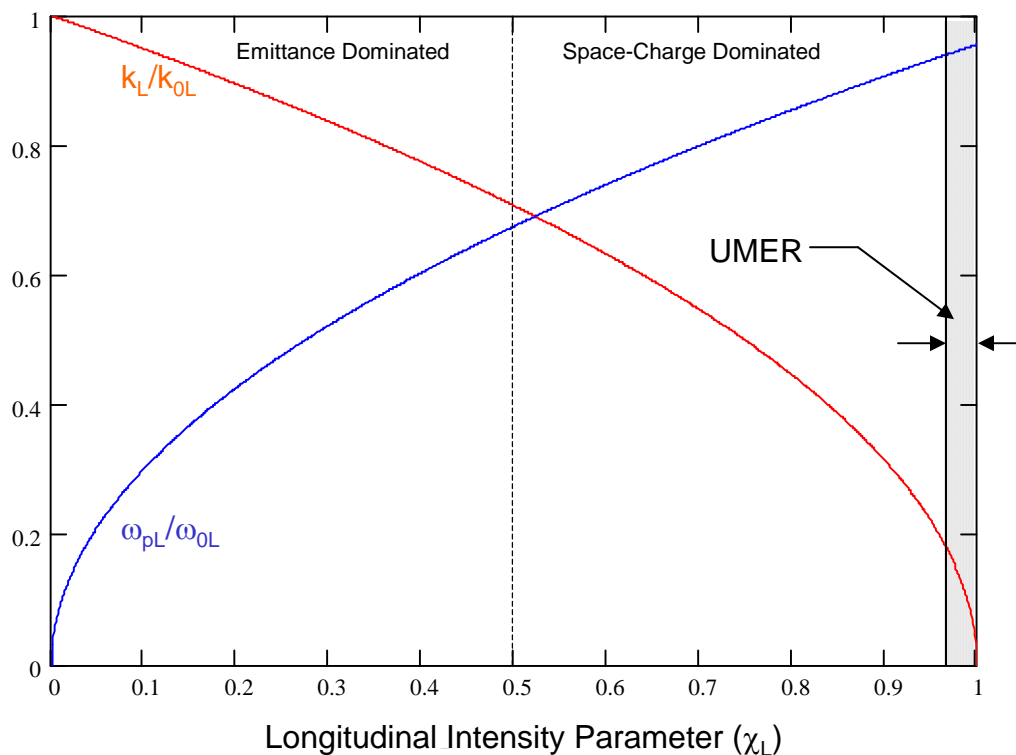


Fig. 3. Longitudinal Space Charge Intensity Parameter (χ_L). This graph relates the intensity parameter for longitudinal beam physics with the longitudinal tune depression (k_L/k_{0L}) and the longitudinal plasma frequency (ω_{pL}). Beams with $0 \leq \chi_L < 0.5$ are considered emittance dominated, while beams with $0.5 < \chi_L \leq 1$ are considered space-charge dominated. Space-charge forces dominate the longitudinal physics of UMER for all practical operating parameters. The operating range for UMER is indicated by the arrows at the extreme right of the graph.

Transverse Envelope Equation

$$R'' + k_0^2 R - \frac{K}{R} - \frac{\varepsilon_x^2}{R^3} = 0$$

Transverse Intensity Parameter

$$\chi = \frac{K}{k_0^2 R^2}$$

Transv. Intensity and Tune Depression

$$\frac{k}{k_0} = \sqrt{1 - \chi}$$

Transv. Intensity and Plasma Frequency

$$\frac{\omega_p}{\omega_0} = \sqrt{2\chi}$$

Longitudinal Envelope Equation

$$z_m'' + \kappa_{z0} z_m - \frac{K_L}{z_m^2} - \frac{\varepsilon_{zz'}^2}{z_m^3} = 0$$

Longitudinal Intensity Parameter

$$\chi_L = \frac{K_L}{k_{0L}^2 z_m^3} = \frac{K_L}{K_L + \left[\frac{\sqrt{5}}{\beta^2 \gamma^3} \frac{\Delta \tilde{E}}{mc^2} \right]^2 z_m}$$

Long. Intensity and Tune Depression

$$\frac{k_L}{k_{0L}} = \sqrt{1 - \chi_L}$$

Long. Intensity and Plasma Frequency

$$\frac{\omega_{pL}}{\omega_{0L}} = \sqrt{\sqrt{\frac{5}{6}} \chi_L} \approx \sqrt{0.91 \chi_L}$$

Table 2. Comparison of longitudinal and transverse relations.

neglected, and it can be rewritten as

$$\left(\frac{d\tilde{z}}{ds}\right)^2 = -\frac{2K_L}{5\sqrt{5}\tilde{z}} + c_1, \quad (26)$$

where the square of the initial rate of expansion $\left(\left[\frac{d\tilde{z}}{ds}\right]_{\tilde{z}_0, s_0}\right)^2$ and the initial value of the

space charge term $\frac{2K_L}{5\sqrt{5}\tilde{z}_0}$ have been summed to form the constant c_1 . The non-RMS

half length z_m is more intuitive, and the need to use RMS values decreases when the emittance is ignored. Therefore, eq. (26) can be rewritten as

$$\left(\frac{dz_m}{ds}\right)^2 = -\frac{2K_L}{z_m} + \frac{2K_L}{z_{m0}} + \left(\left[\frac{dz_m}{ds}\right]_{z_{m0}, s_0}\right)^2. \quad (26a)$$

Taking the square root of eq. (26a) gives

$$\frac{dz_m}{ds} = \pm \sqrt{-\frac{2K_L}{z_m} + \frac{2K_L}{z_{m0}} + \left(\left[\frac{dz_m}{ds}\right]_{z_{m0}, s_0}\right)^2}, \quad (27)$$

which can be directly integrated to find $s(z_m)$:

$$s = s_0 + \left[\pm \frac{\sqrt{c_1 z_m^2 - 2K_L z_m}}{c_1} \pm \frac{K_L}{c_1^{3/2}} \ln \left| 2\sqrt{c_1} \sqrt{c_1 z_m^2 - 2K_L z_m} + 2c_1 z_m - 2K_L \right| \right]_{z_{m0}}^{z_m}. \quad (28)$$

Note that the rates of expansion $\left[\frac{dz_m}{ds}\right]_{z_{m0}, s_0}$ and $\frac{dz_m}{ds}$ in eq. (26a) are squared, destroying

some information about the beam. To counteract this, the \pm sign is introduced when the

square root is taken in eq. (27). In eq. (28), the upper sign is taken when $\frac{dz_m}{ds} \geq 0$, and

the lower sign is taken when $\frac{dz_m}{ds} \leq 0$.

Referring to Fig. 4, note that $\frac{dz_m}{ds} = 0$ only when the beam is at a longitudinal "waist," or local minimum length. By assuming this condition in eq. (26a), and entering the full expression for c_1 , an expression for the non-RMS minimum half length of a space-charge dominated beam undergoing contraction in the absence of external longitudinal focusing is found to be

$$z_{mw} = \frac{2K_L}{\frac{2K_L}{z_{m0}} + \left(\left[\frac{dz_m}{ds} \right]_{z_{m0}, s_0} \right)^2}. \quad (29)$$

The longitudinal envelope calculated in eq. (28) for the UMER beam undergoing free expansion is shown in Fig. 6. Note that the independent variable in eq. (28) is the distance traveled by the beam center, s , and the dependent variable is the non-RMS half-length of the beam, z_m , so when $\frac{dz_m}{ds} \rightarrow 0$, $\frac{ds}{dz_m} \rightarrow \infty$, and the graphing program will not plot the curve in its entirety. However, the curves in these regions can be found by simply extrapolating the plotted curves. Note also that the length referred to in Fig. 6 is the non-RMS full length, which is greater than the RMS half-length \tilde{z} by a factor of $2\sqrt{5}$.

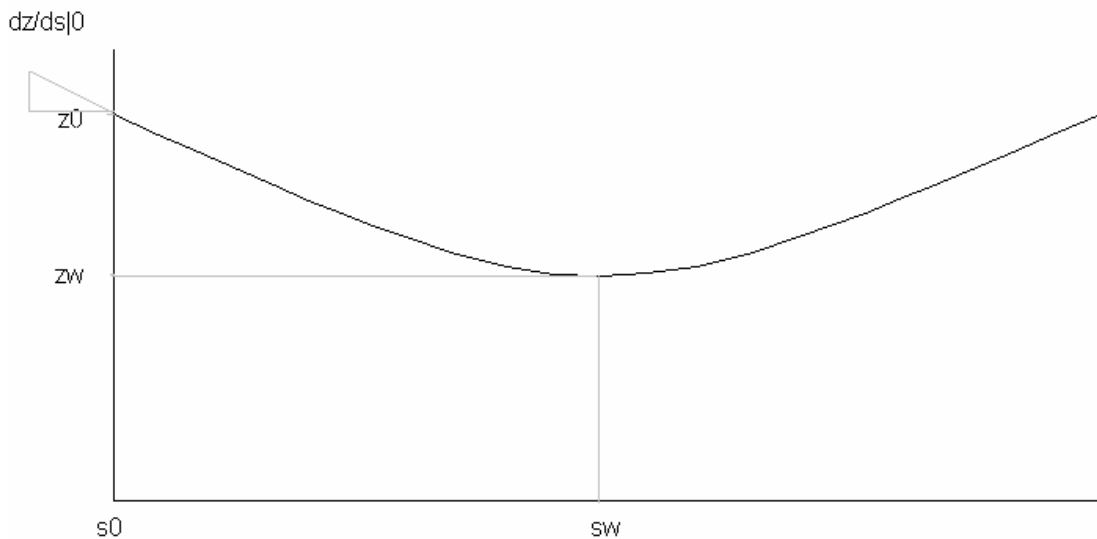


Fig. 4. Longitudinal envelope for a beam with initial half-length z_0 and initial slope $\left[\frac{dz}{ds}\right]_0$, and with a "waist" of half-length z_w when the beam center is located at s_w .



Fig. 5. This figure shows a beam which is in the process of formation but which has an initial contraction ($\left[\frac{dz}{ds}\right]_0 < 0$) due to a velocity tilt imposed at the cathode.

K represents the location of the cathode. The length of the overall line represents the length of the beam which is taken into account by the theory. Although only the portions of the lines to the right of the cathode actually exist, this is not accounted for by the theory. Thus, it is possible to discuss a beam which is contracting even though it is in the process of creation at the cathode, and the overall length of the beam is increasing.

2.4. Longitudinal Focusing for Parabolic Beams.

The longitudinal envelope equation can also be used to consider a beam where longitudinal focusing is present. For this, we return to eq. (25). If the beam is space-charge dominated, the emittance term can be neglected, and eq. (25) can be rewritten as

$$\left(\frac{d\tilde{z}}{ds}\right)^2 = -\frac{2K_L}{5\sqrt{5}\tilde{z}} - \kappa_{z0}\tilde{z}^2 + c_2, \quad (30)$$

where

$$c_2 = \frac{2K_L}{5\sqrt{5}\tilde{z}_0} + \kappa_{z0}\tilde{z}_0^2 + \left(\left[\frac{d\tilde{z}}{ds}\right]_{\tilde{z}_0, s_0}\right)^2. \quad (31)$$

Integration can be performed on eq. (30) to find the longitudinal envelope in the form

$s(\tilde{z})$:

$$s = s_0 + \int_{\tilde{z}_0}^{\tilde{z}} \frac{\tilde{z}}{\pm \sqrt{-\frac{2K_L\tilde{z}}{5\sqrt{5}} - \kappa_{z0}\tilde{z}^4 + c_2\tilde{z}^2}}. \quad (32)$$

The choice of sign depends on whether the beam is undergoing contraction or expansion.

If the electric field applied at each gap was known as a function of time, $\kappa_{z0}(s, t)$ could be determined, and the longitudinal envelope found directly from eq. (32). However, since the goal is to determine the fields needed, the use of eq. (32) is not the most efficient method.

The geometry of the UMER focusing lattice, which was decided early in its development, poses a constraint on the design of the longitudinal focusing system (Fig. 7). The longitudinal focusing lattice consists of three locations in the ring which are available for use by the induction gaps. These locations are equally spaced along the ring, with the

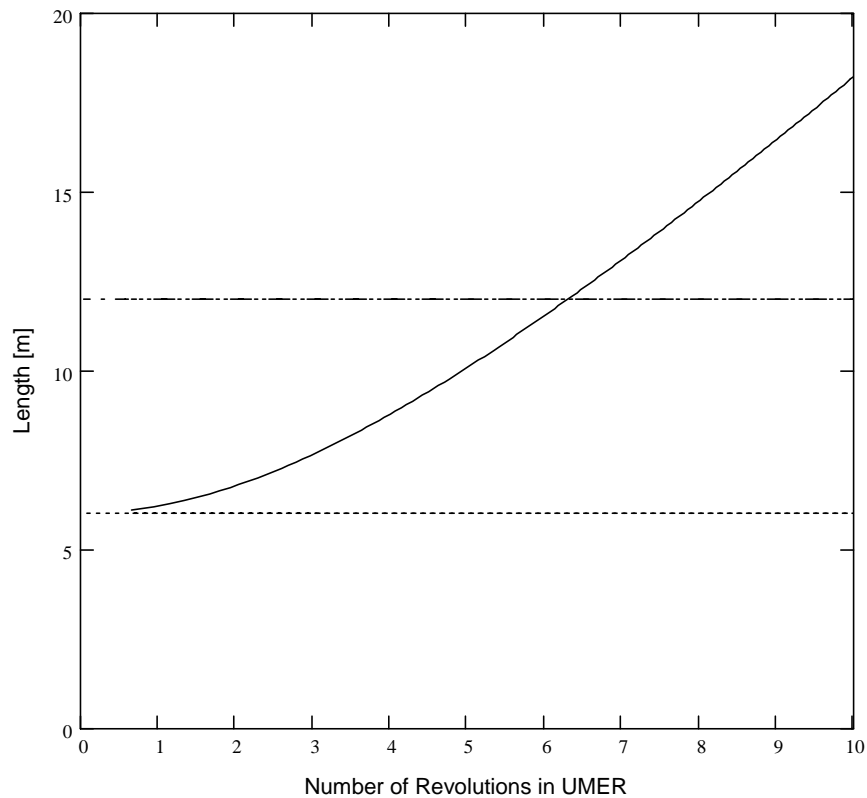


Fig. 6. Expansion of Parabolic Beam, showing that the UMER beam would completely fill the ring after the sixth revolution. Solid curve is full beam length, dotted line is initial full length of beam, and dash-dot line is the circumference of UMER. Note that the expansion becomes linear past about the seventh revolution. Current is 100 mA, pulse length is 100 ns. Injector length is neglected.

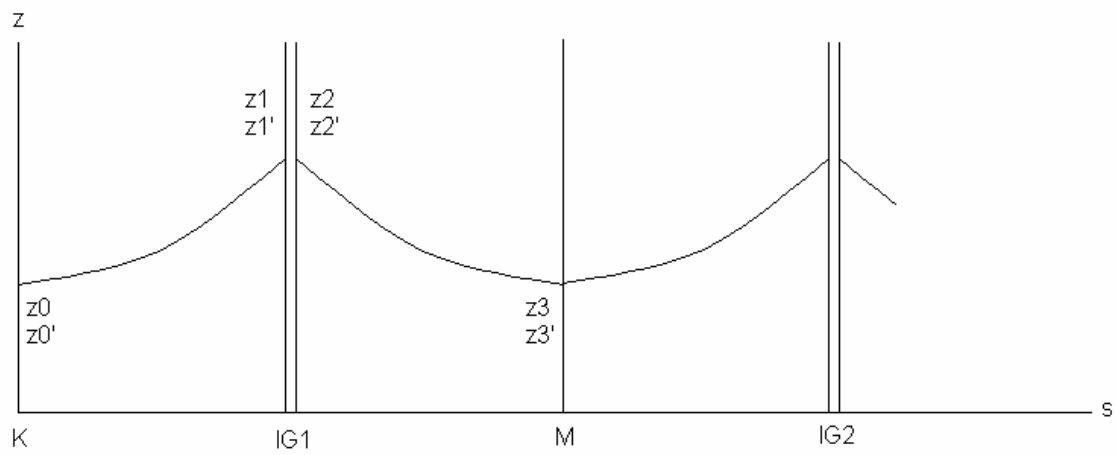


Fig. 7. Longitudinal Focusing Lattice, showing location of cathode K , induction gaps $IG1$ and $IG2$, midpoint between induction gaps M , and longitudinal envelope at each location

first location being about 2 m downstream of the gun, and with a spacing of about 4 m between each location in the ring. This particular geometry is useful because its symmetry can be exploited in simplifying the design of the longitudinal focusing system, and because the results presented below are applicable to any space-charge dominated beam transport system with similar symmetry.

At the cathode (K in Fig. 7), the beam has its initial length \tilde{z}_0 and divergence \tilde{z}'_0 . Between K and the first induction gap (IG1), a distance of about 2 m, the beam has undergone free expansion as given by eqs. (27) and (28), arriving at IG1 with new length \tilde{z}_1 and divergence \tilde{z}'_1 . In the thin lens approximation, the length of IG1 is very small, but not zero. Accordingly, the beam emerges with length

$$\tilde{z}_2 = \tilde{z}_1 + \delta \approx \tilde{z}_1, \quad (33)$$

where δ is small but not zero, and with divergence \tilde{z}'_2 given by eq. (30). If the focusing effects of IG1 have totally overcome the space-charge-driven expansion of the beam, the beam will begin to contract, arriving at the midpoint between the gaps (M) with a new length \tilde{z}_3 and divergence \tilde{z}'_3 . If $\tilde{z}_3 = \tilde{z}_0$ and $\tilde{z}'_3 = \tilde{z}'_0$, and if the internal structure, entropy, etc., of the beam have remained approximately unchanged, the envelope from M to IG2 should be identical to the envelope from K to IG1. The fluid-analogy equations which govern changes in the beam are time-reversible[7,20], so we expect that we can produce conditions at M which are identical to those at K provided that $\tilde{z}_1 = \tilde{z}_2$ and $\tilde{z}'_1 = -\tilde{z}'_2$. Since the former condition is approximately fulfilled simply by the short length of the induction gap, the problem is to find the focusing strength at IG1 which will result in $\tilde{z}'_1 = -\tilde{z}'_2$. From eqs. (30) and (31),

$$\tilde{z}_2' = -\sqrt{\frac{-2K_L}{5\sqrt{5}\tilde{z}_2} - \kappa_{z0}\tilde{z}_2^2 + \frac{2K_L}{5\sqrt{5}\tilde{z}_1} + \kappa_{z0}\tilde{z}_1^2 + \tilde{z}_1'^2}. \quad (34)$$

The negative sign was chosen because the beam is undergoing focusing, and therefore

$\tilde{z}_2' < \tilde{z}_1'$. For $\tilde{z}_1' = -\tilde{z}_2'$,

$$\frac{-2K_L}{5\sqrt{5}\tilde{z}_2} - \kappa_{z0}\tilde{z}_2^2 + \frac{2K_L}{5\sqrt{5}\tilde{z}_1} + \kappa_{z0}\tilde{z}_1^2 = 0. \quad (35)$$

Combining eqs. (33) and (35) gives

$$-2\frac{K_L}{5\sqrt{5}} = -2\kappa_{z0}\tilde{z}_1^3 - 3\kappa_{z0}\tilde{z}_1^2\delta - \kappa_{z0}\delta^2\tilde{z}. \quad (36)$$

Taking the limit of eq. (36) as $\delta \rightarrow 0$ gives

$$\kappa_{z0} = \frac{K_L}{5\sqrt{5}\tilde{z}_1^3}, \quad (37)$$

the approximate focusing strength needed to achieve a stable longitudinal focusing lattice for a parabolic beam in UMER as shown in Fig. 7.

A critical step in this calculation was the assumption that the length of the first induction gap was small *but not zero*. If its length were zero, the beam would be inside the gap for no period of time, meaning that no focusing would occur, and the beam properties before and after the first induction gap would be identical. Since the gap length is not zero, the gap is able to apply focusing forces to the beam, causing it to begin to contract. However, since the gap length is small, the beam length will only have changed by a very small amount, δ , during its transit of the gap. Thus eq. (35) is a meaningful, nontrivial expression allowing us to calculate the focusing constant in the *limit* of the thin lens approximation.

However, this does not take into account the relative lengths of the induction gap and the focusing period. To account for this, eq. 37 must be multiplied by the ratio of the focusing period to the gap length:

$$\kappa_{z0} = \frac{K_L}{5\sqrt{5}\tilde{z}_1^3} \frac{L_{period}}{L_{gap}}. \quad (37a)$$

Although this does not arise naturally out of the above treatment, it must be included to obtain the correct results.

From the expression for the focusing constant in eq. (37a), the actual electric field strength needed to properly focus a parabolic beam in UMER can be calculated. The focusing constant itself is defined in terms of the applied electric field gradient in

z , E'_{az} [12]:

$$\kappa_{z0} = \frac{qE'_{az}}{mc^2\beta^2\gamma^3}. \quad (38)$$

In this case the prime denotes a derivative with respect to z , the distance in the beam frame where $z = 0$ at the beam center. The applied electric field along z can also be written in terms of E'_{az} :

$$E_{az} = \int E'_{az} dz = \int \frac{dE_{az}}{dz} dz. \quad (39)$$

Solving for E'_{az} in eq. (38) and using eq. (39),

$$E_{az} = \frac{mc^2\beta^2\gamma^3}{q} \int \kappa_{z0} dz. \quad (40)$$

From the relation between the focusing constant and the longitudinal perveance in eq. (37),

$$E_{az} = \frac{mc^2 \beta^2 \gamma^3}{q} \int_{z_0}^z \frac{K_L}{5\sqrt{5}\tilde{z}_1^3} \frac{L_{period}}{L_{gap}} dz. \quad (41)$$

Since \tilde{z}_1 is the actual RMS half length of the beam before it enters the first induction gap, it is not included in the integration, which yields

$$E_{az} = \frac{mc^2 \beta^2 \gamma^3}{q} K_L \frac{L_{period}}{L_{gap}} \frac{z - z_0}{z_{m1}^3}, \quad (42)$$

where $z_{m1} = \sqrt{5}\tilde{z}_1$ is the non-RMS half length of the beam before it enters the first induction gap, z is the location in the beam at which the field E_{az} is applied, and $z_0 = 0$ is the center of the beam. Eq. (42) can be further described in terms of fundamental quantities by using the definition of longitudinal perveance from eq. (3):

$$E_{az} = \frac{3}{2} \frac{gNq}{4\pi\epsilon_0\gamma^2} \frac{L_{period}}{L_{gap}} \frac{z}{z_{m1}^3}. \quad (43)$$

The applied focusing field can be written in terms of the electric field due to space charge,

$$E_{sz} \approx \frac{-g}{4\pi\epsilon_0\gamma^2} \frac{\partial\lambda}{\partial z}, \quad (44)$$

where g is a geometry factor. Eq. (44) is only exact for certain distributions[12], but is

approximately true for any distribution in the special case where $\frac{\partial\lambda}{\partial z}$ is small[21]. The

geometry factor g depends on beam radius, beam pipe radius, beam length, and location in the beam[12]. The exact value of g must be calculated numerically. For beams whose length is much greater than the beam pipe radius, an average value for g is given approximately by

$$g \approx \alpha + 2 \ln\left(\frac{b}{a}\right), \quad (45)$$

where a is the beam radius, b is the beam pipe radius, and α is a constant. The value of α is generally given as one[21], but other values have been proposed. Where beam variation is slow[22,23], near the center of a long beam[12], or where the longitudinal electric field is being measured on the beam surface[7], α has been given as zero. When g is averaged over the entire beam cross section, α has been given as 0.67[12] or 0.5[7,24,25]. Other authors indicate that g , and therefore α , is independent of radial position[20,23]. An experiment carried out by D.X. Wang at the University of Maryland found $\alpha = 0.01 \pm 0.16$ [7]. These values are clearly inconsistent, and additional work is needed to determine the best value for α .

Using eqs. (43) and (44), and assuming the parabolic line charge density of eq. (16), the applied field can be related to the space-charge field by

$$E_{az} \approx \frac{3Nq}{4\lambda_0 z_{m1}} \frac{L_{period}}{L_{gap}} [E_{sz}]. \quad (46)$$

Note that eqs. (42) and (43) are linear in z , which is expected since the beam pulse shape is parabolic. Also note that the applied field needed to properly focus a parabolic beam in the UMER lattice is proportional to the longitudinal perveance (and therefore increases with space charge), and depends (slowly) on the ratio of beam diameter to beam pipe diameter through the geometry factor g .

2.5. Limitations.

Although the longitudinal envelope equation is directly useful in describing the behavior of parabolic beams, and in describing some fundamental behavior of

nonequilibrium¹ equivalent beams, it does have limitations. The longitudinal envelope equation does not directly give detailed information about the velocity distribution and line charge density in non-parabolic beams, which are necessary to design focusing systems for those beams. Also, the longitudinal envelope equation is not the best format for describing the propagation of longitudinal space-charge waves.

¹ The equilibrium distribution is the Boltzmann profile, which is parabolic for zero longitudinal temperature and Gaussian for high longitudinal temperature. This distribution retains its shape during expansion[16].

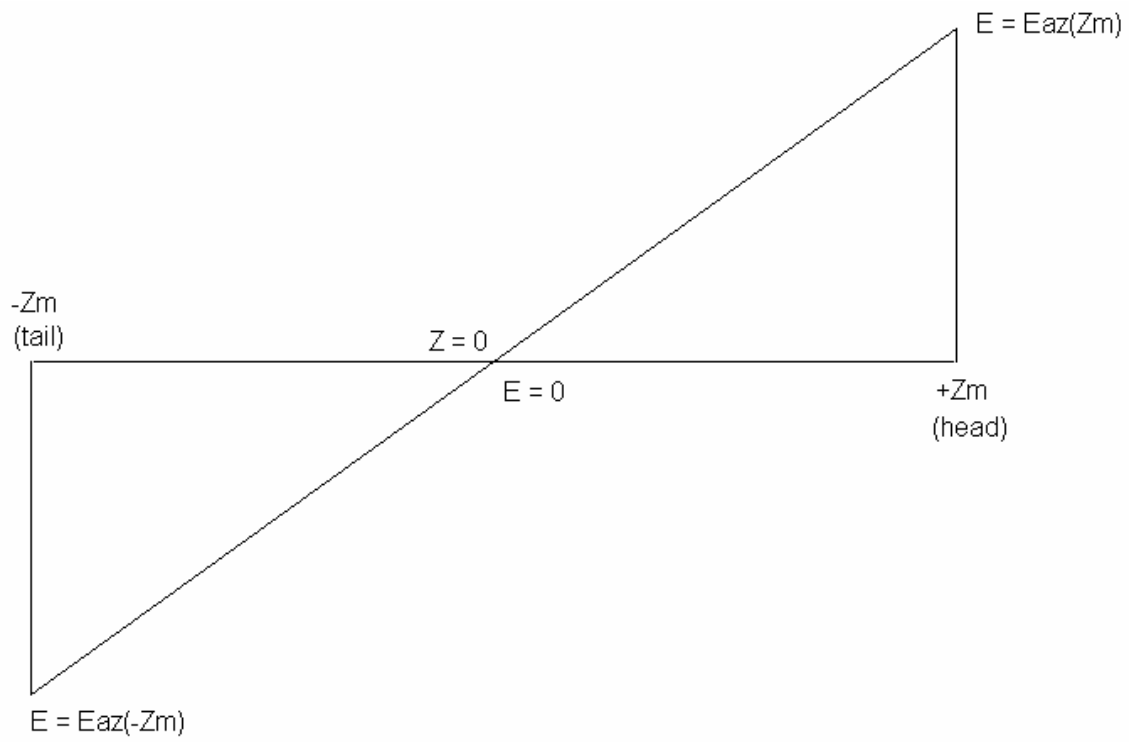


Fig. 8. Applied electric field for focusing of parabolic beam in stable UMER longitudinal focusing lattice.

3. One-Dimensional Cold Fluid Model.

3.1. Introduction.

The longitudinal envelope equation is a frequently used model for the longitudinal behavior of space-charge dominated beams. However, this model has limitations and is not useful in all cases. An alternate model, the cold-fluid model, makes use of the fact that the equations governing the behavior of space-charge dominated beams are similar to those governing cold, compressible fluids. One application of this model which is particularly important is to the expansion of an initially rectangular beam. This line charge profile is useful because its flat top could allow better measurements of space charge waves[26] and could provide the constant impedance necessary for induction linacs[16]. In this section the governing equations are introduced and results are given for the special case of an expanding, initially rectangular beam.

3.2. Governing Equations.

For a space-charge dominated beam undergoing free expansion, it is possible to write two equations which govern the behavior of the particles in the beam. The first is the continuity equation

$$\frac{\partial \rho}{\partial t} + \vec{\nabla} \cdot \vec{J} = 0, \quad (47)$$

which relates the volume charge density ρ and the current density \vec{J} , and which can be derived directly from Maxwell's Equations[27]. If all behavior being considered is strictly longitudinal (along \hat{z}) and if the beam has a constant cross-sectional area A , the line charge density $\lambda = A\rho$, and the continuity equation can be rewritten in its one-dimensional form

$$\frac{\partial \lambda}{\partial t} + \frac{\partial}{\partial z} v \lambda = 0, \quad (48)$$

since $\vec{J} = \rho \vec{v}$.

The longitudinal force exerted on a particle in a space-charge dominated beam undergoing free expansion is strictly due to space charge. This field is taken as

$$E_{sz} \approx -\frac{g}{4\pi\epsilon_0\gamma^2} \frac{\partial \lambda}{\partial z}. \quad (49)$$

The acceleration of particles in the beam has two physical origins: a stationary term $v \frac{dv}{dz}$

due to variation of the flow as particles pass through regions with different properties;

and a nonstationary term $\frac{dv}{dt}$ which describes changes in the flow at any given

location[28]. Thus

$$\frac{F}{m} = \ddot{z} = \frac{\partial v}{\partial t} + v \frac{\partial v}{\partial z} = \frac{e}{m\gamma^3} E_{sz}. \quad (50)$$

Taking into account the approximate expression for space charge field given in eq. (49),

$$\frac{\partial v}{\partial t} + v \frac{\partial v}{\partial z} \approx -\frac{qg}{4\pi\epsilon_0 m \gamma^5} \frac{\partial \lambda}{\partial z}. \quad (51)$$

This equation is known as the momentum equation[7,24]. The momentum equation and the one-dimensional continuity equation together fully describe the particle flow in one-dimensional cold beams in most cases. In compressible fluid flow, the momentum equation is replaced by the analogous Euler equation

$$\frac{\partial v}{\partial t} + v \frac{\partial v}{\partial z} \approx -\frac{1}{\rho} \frac{\partial p}{\partial z}, \quad (52)$$

where p is pressure and ρ is volume mass density. Bernoulli's equations for compressible and incompressible flow can be derived from this equation[28].

3.3. Rectangular Beam Expansion and the Method of Characteristics.

One method of finding solutions to the momentum and continuity equations which was first developed for supersonic gas flow and which has been used by the beam physics community for some time is the method of characteristics[29-31]. In the method of characteristics, incremental changes in the fluid propagate through it as waves. One application of the method of characteristics to beams is to the evolution of an initially rectangular beam pulse. This solution is given elsewhere[7,24], and will not be repeated in depth here, although the underlying physical behavior will be discussed in general terms and its results will be given below.

For longitudinal focusing, it is important to understand the source of the beam expansion. Consider the edge of a rectangular beam. Inside the beam, far from the edge, the electric fields experienced by a charge tend to cancel, since there are opposite contributions from particles to the left and right of the particle under consideration. At the edge, there will be a net field, since the contributions of charges to one side are not balanced by contributions of charges from the other side. This results in a net force on charges near the edge of the beam, causing them to accelerate outward from the beam, causing the beam to expand.

Although this picture provides a rough understanding of the physics of beam expansion, it does not immediately give a numerical description of the expansion. For this quantitative understanding, we turn to the fluid analogy and the phenomenon of cavitation. Consider an infinitely long pipe, filled with a fluid which is confined to $z \leq 0$

by a massless piston at $z = 0$ (Fig. 9). At $t = 0$, this phantom piston is moved towards the right at infinite speed. Since the fluid consists of real, massive particles, it can only adjust to the new configuration at finite speed. The fluid will adjust by producing two waves, one which travels into the body of the gas at the speed of sound in the gas, and the other which travels outward into the vacuum at a maximum speed, called the escape speed. The speed of sound in a charged particle beam is given by[7,20]

$$c_0 = \sqrt{\frac{Zqg\lambda_0}{4\pi\epsilon_0 m\gamma^5}}, \quad (53)$$

where Z is the charge state of the particles in the beam, q is the fundamental charge, and m is the mass of the particles in the beam. For a 100 mA electron beam with $g = 2.8$ and $\beta = 0.2$, $c_0 = 2.59 \times 10^6 \frac{m}{s}$. The escape speed is given by[30]

$$\left| \left(\frac{u}{c_0} \right)_{\max} \right| = \frac{2}{k-1}$$

or

$$u_{\max} = \frac{2}{k-1} c_0, \quad (54)$$

where $k = 2$ for an electron beam[20]. Thus, the escape speed, also the speed of the expanding edge, is

$$u_{\text{edge}} = 2c_0. \quad (55)$$

This treatment is not valid at very low pressures, but it is appropriate for beams like that produced in UMER, since the fluid analogy of space-charge dominated beams are cold, high-pressure gasses.

This situation is identical to that of a beam which has just been produced at the cathode. In that case, the flat top will shrink from each end with the speed of sound, while the beam will expand outward from each end with twice the speed of sound.

Further explanation of the behavior of an expanding, initially rectangular space-charge dominated beam can be found by using the full method of characteristics to find $\lambda(z,t)$ and $v(z,t)$. When this is done, the following results are obtained:

$$\text{Zone I (Dead Zone)} \quad \lambda = \lambda_0 \quad (56a)$$

$$v = v_0 = 0 \quad (56b)$$

$$\text{Zone II (Rarefaction Zone)} \quad \lambda(z,t) = \left(\frac{2}{3} \pm \frac{1}{3} \frac{z - z_0}{tc_0} \right)^2 \lambda_0 \quad (56c)$$

$$v(z,t) = \frac{2}{3} \left[\frac{z - z_0}{t} \mp \sqrt{\frac{Zeg}{4\pi\epsilon_0 m} \lambda_0} \right] \quad (56d)$$

$$\text{Zone III (Vacuum)} \quad \text{no fluid present}$$

In eqs. (56), λ_0 is the initial line charge density of the rectangular pulse, v_0 is the initial velocity (in the beam frame) of the particles in the beam, which is taken to be zero, z is the location in the beam with $z = 0$ at the beam center, z_0 is the initial location of the front or rear edge of the beam, and t is the time measured from $t = 0$ when the phantom piston is removed. The \pm and \mp signs refer to the fact that there are two rarefaction zones, one formed by the erosion of the flat top from the front edge of the beam, and one formed by the erosion of the flat top from the rear edge of the beam. The upper sign is used when the erosion is from the rear edge, and the lower sign is used if the erosion is from the front edge. The equations presented above are only valid so long as the two

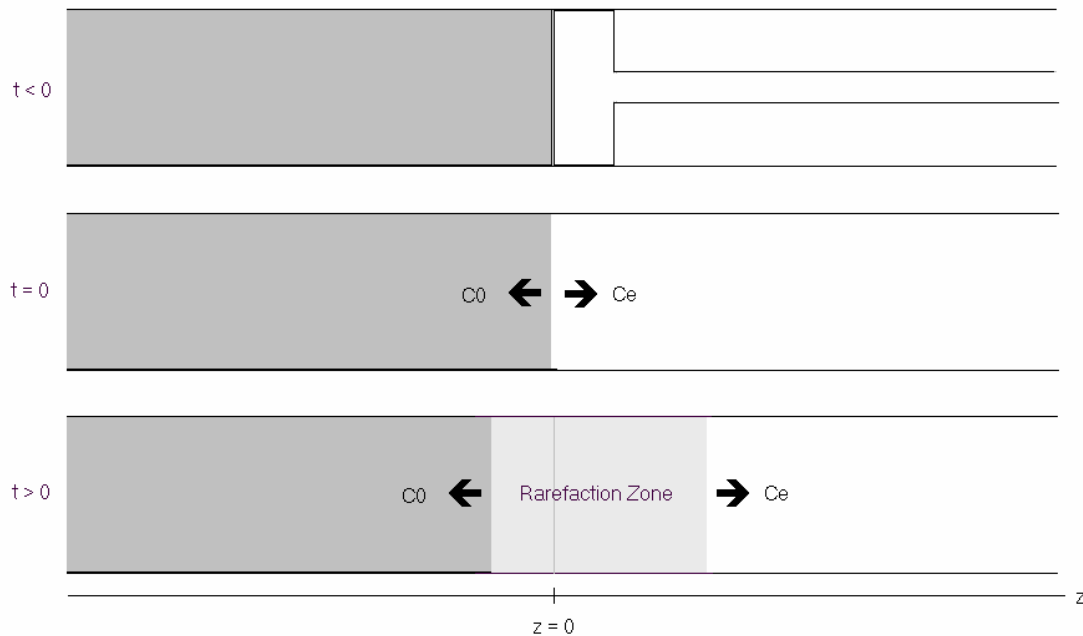


Fig. 9. Fluid Analogy for expansion of rectangular electron beam. Gas is initially at rest, confined to $z < 0$. At $t = 0$, massless piston is removed to the right at infinite speed. Shockwaves propagate into the gas at the speed of sound c_0 , and into the vacuum at escape speed c_e , forming a rarefaction zone where the compressible fluid is present but at lower density than in the undisturbed region to the left of the left going shockwave.

rarefaction zones have not connected. At this point, the flat top has been eliminated, and the beam is "all edges." A cusp will occur at the middle of the beam where the slope of the line charge density abruptly changes. After this time, the shock waves which caused the flat top to erode begin to overlap, and the resulting nonlinear equations cannot be solved exactly. An approximate solution is given elsewhere[7,20]. However, for the purposes of establishing a stable longitudinal focusing lattice, it is desirable to prevent the beam from reaching the cusp point, for reasons addressed in section 4.3. For a 100 mA electron beam with $g = 2.8$ and $\beta = 0.2$, and an initial full length of 6 m the cusp will occur after 1.16 μs . By this time the beam center will have traveled 69.6 m, and the new full length of the beam will be 18 m.

3.4. Coherent Energy Spread.

Coherent energy spread, the difference in kinetic energy between the fastest particle and the slowest particle in the beam, is an important consideration in the design of focusing systems. In the expanding rectangular pulse, the particles at the extreme head and extreme tail are expanding away from the center of the beam (in the beam frame) at the escape velocity $2c_0$. The energies of particles at the beam center, at the extreme head, and at the extreme tail can be calculated nonrelativistically in the laboratory frame as

$$T_{center} = \frac{1}{2} m(c\beta)^2,$$

$$T_{head} = \frac{1}{2} m(c\beta + 2c_0)^2,$$

and

$$T_{tail} = \frac{1}{2}m(c\beta - 2c_0)^2.$$

Nonrelativistically, the kinetic energy of the center particle in an electron beam traveling at $\beta = 0.2$, measured in the laboratory frame, is 10.2 keV. If the initial beam current is 100 mA, and $g = 2.8$, the energy of the particle at the extreme head of the beam, corresponding to its escape velocity, will be 12.1 keV, while the energy of the particle at the extreme tail of the beam will be 8.5 keV, for an extreme coherent energy spread of 3.6 keV. This calculation was repeated for an experiment currently being performed by Yupeng Cui at the University of Maryland. In that experiment, the nominal electron beam energy is 5 keV, the actual beam center energy is 4.897 keV, the beam current is 135 mA, and the geometry factor is approximately 3.7. The speed of sound in the beam, calculated using eq. (53), is $4.22 \times 10^6 \frac{m}{s}$. The kinetic energy of the particle at the extreme head of the beam, T_{head} , is 7.014 keV. Simulations performed by Yupeng Cui[32] using the WARP 3D simulation code indicate that the kinetic energy of the particle at the extreme head is 7.109 keV, which indicates only a 1.34% difference between the one-dimensional theory and the three-dimensional simulation.

The particles at the extreme head and extreme tail of the beam will never increase their velocity. Since the expansion speed, and therefore the coherent energy spread, cannot be changed without changing the initial line charge density, it is more proper to think about the number of particles in the edges as opposed to the extreme coherent energy spread. Due to the transverse focusing system, particles whose energies are different from the beam's design energy will be mismatched. For particles whose energy falls within a certain range, their trajectories will simply differ from the design orbit of

the machine. If their energies fall outside that range, their trajectories will be so different from the design orbit of the machine that they will be lost to the wall. Because there will always be some particles traveling at the escape speed, if the escape speed is higher than the critical energy at which a particle is misfocused into the wall, there will be some particles lost from the beam. However, the number of particles lost by the beam will depend on how many have achieved velocities in excess of the critical velocity, which depends directly on how long the beam has been propagating. Therefore, although particle loss may not be avoidable, it is possible to limit the number of particles lost by applying longitudinal focusing to limit the length of the edge regions, and therefore the number of particles with an energy above the critical energy.

3.5. Discrepancies.

Some simulations and experiments have been conducted to determine whether a rectangular, space-charge dominated beam erodes according to the results of the cold fluid model, notably by D.X. Wang at the University of Maryland[7], and by A. Faltens at Lawrence Berkeley Laboratory[24]. Experimental data produced by Faltens and Wang agrees well with simulations performed by Wang. Recent simulations, which were performed using the WARP simulation code for space-charge dominated beams, are also in good agreement. These simulations and experiments uniformly show a line charge density which is qualitatively different from, but quantitatively similar to, the line charge density determined from the cold fluid model. Specifically, simulations and experiments indicate that the transition from the flat top to the edge is not abrupt as shown in Fig. 10, but more gradual. The magnitude of the discrepancy is small enough that it was not even mentioned by Wang and Faltens, but the fact that it appears consistently in two

independent experiments and two independent simulations suggests it is more than mere experimental error. Although the source of this rounding is not yet understood, several assumptions of the cold fluid model are not exactly correct and may be to blame. For example, the space charge field given in eq. (44) is only correct for a slowly-varying line charge, which is not the case early in the evolution of a rectangular beam pulse. In addition, the cold fluid model assumes that all effects are one-dimensional while the actual beam is a three-dimensional object. This discrepancy is currently under investigation.

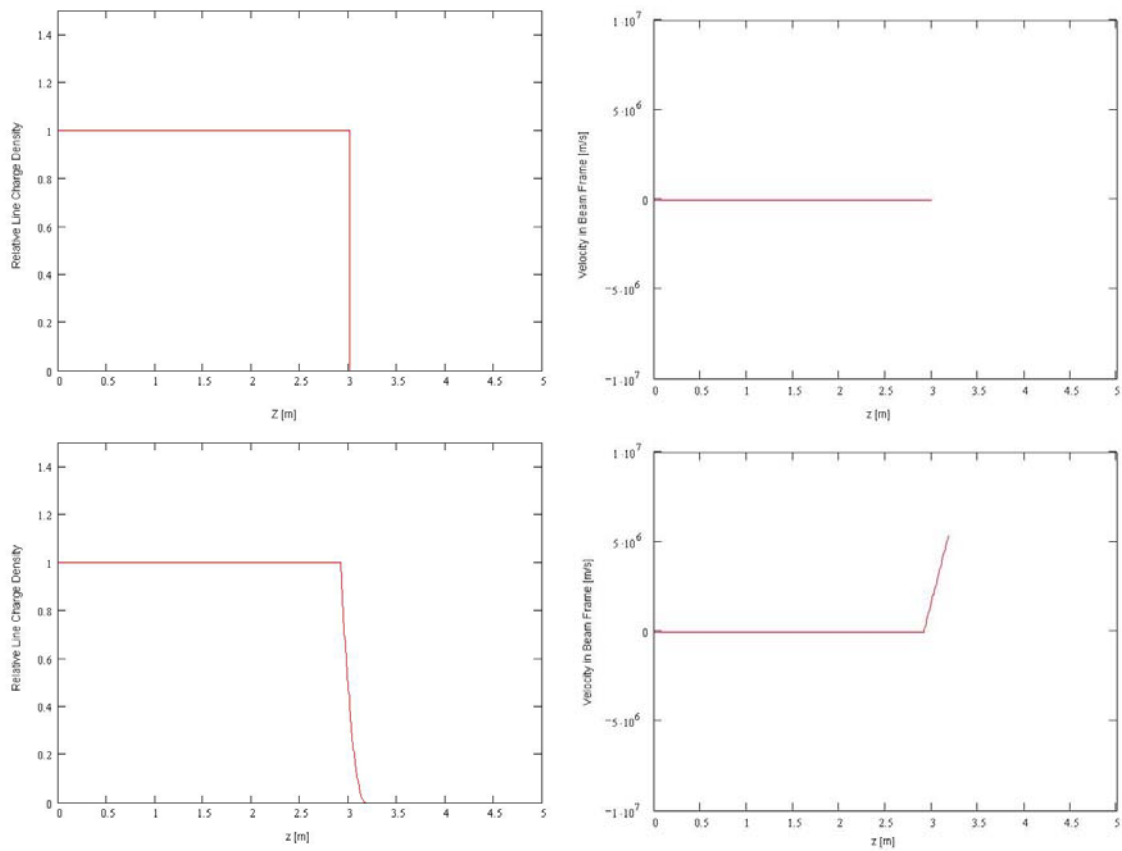


Fig. 10 (a - d). Line charge density (left) and electron velocity in the beam frame (right) for the front half of the beam, measured at $s = 0$ m (top) and $s = 2$ m (bottom). Graphs at 0 m correspond to initial conditions at cathode, while graphs at 2 m correspond to conditions at first induction gap. Beam parameters: 100 mA current, 100 ns initial full pulse length, $\beta = 0.2$, $g = 2.86$.

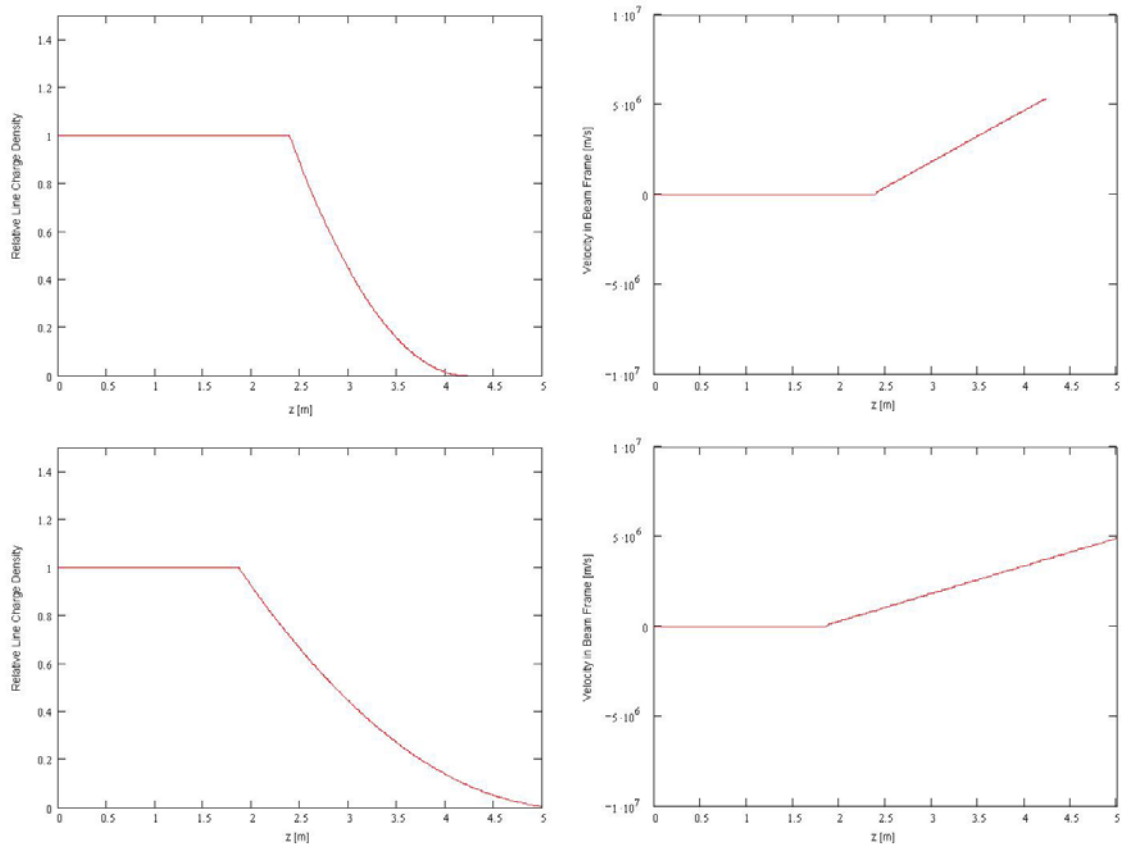


Fig. 10 (e - h). Line charge density (left) and electron velocity in the beam frame (right) for the front half of the beam, measured at $s = 14$ m (top) and $s = 26$ m (bottom). Graphs at 14 m correspond to conditions after injection and one revolution without focusing, while graphs at 26 m correspond to conditions after injection and two revolutions without focusing. Beam parameters: 100 mA current, 100 ns initial full pulse length, $\beta = 0.2$, $g = 2.86$.

4. Longitudinal Focusing in UMER: A more general approach.

4.1. Introduction.

The one-dimensional cold fluid model is particularly useful for designing longitudinal focusing systems because it gives detailed information about the velocities of particles in the beam and the line charge density of the beam as the beam travels through the transport system. This information, along with the periodicity of the longitudinal focusing system in UMER, can be exploited to calculate the necessary longitudinal focusing field in a more general way than was presented in connection with the longitudinal envelope equation. The method described below has two advantages: as input it requires only $v(z)$ and $\lambda(z)$ at the location of the gap, which can be found through any means, be it theory, simulation, or experiment; and it is applicable to any space-charge dominated beam transport system exhibiting a longitudinal focusing system with periodicity similar to UMER.

4.2. Longitudinal Focusing.

As the beam expands from its initial length at the cathode, its line charge and the velocity distribution of its particles will change. For some initial conditions, such as the rectangular beam, these properties can be calculated. For other initial conditions, it may be difficult to calculate these properties, and simulations must be used. In a longitudinal focusing lattice (Fig. 7), this expansion will proceed until the first induction gap has been reached, at which point some electric field, which may vary in time, is applied to the beam. Because the momentum and continuity equations are time reversible[7,20], it should in principle be possible to reverse the beam's expansion by reversing the velocity (in the beam frame) of every particle in the beam by applying a carefully tailored electric

field at the first induction gap. This converts the beam's expansion into contraction. Because this contraction is the mirror image of the beam's earlier expansion, it will reach a waist where the beam properties are identical to those at the cathode (assuming entropy does not increase). Thus the expansion from this waist to the second induction gap is identical to the expansion from the cathode to the first gap. Each expansion, each contraction, and each induction gap pulse will be identical if the velocity reversal is done perfectly.

The task is now to determine what electric field should be applied to reverse the velocity of each particle in the beam. Assume a beam of half-length z_h , centered at the origin in its rest frame. A planar diode, with a hole in its center, will serve as a model for the induction gap. The diode has a gap length l . An electric field $E(t)$, which is uniform in space but variable in time, can be applied across the gap. The entire diode is traveling with velocity $-c\beta$ in the rest frame of the beam. As the diode moves past the beam, each point in the beam is exposed to the field in the gap ($E(t)$) for $\frac{l}{c\beta}$ seconds.

$E(t)$ varies slowly enough that the field applied to any particle is approximately constant during its passage through the gap. Because the beam consists of electrons, an impulse I is applied to each particle as it passes through the gap:

$$I = F\Delta t = q[E_{net}] \frac{l}{c\beta} = q \left[E_{sz}(z) - E \left(\frac{z_h - z}{c\beta} \right) \right] \frac{l}{c\beta} = \Delta p = m\Delta v. \quad (57)$$

Note that this equation is nonrelativistic, so only the particles' velocities are affected, not their effective masses. The location of the gap ($z = z_h - c\beta t$) in the beam frame has been used to describe the applied electric field in terms of spatial coordinates. $E_{sz}(z)$ is the

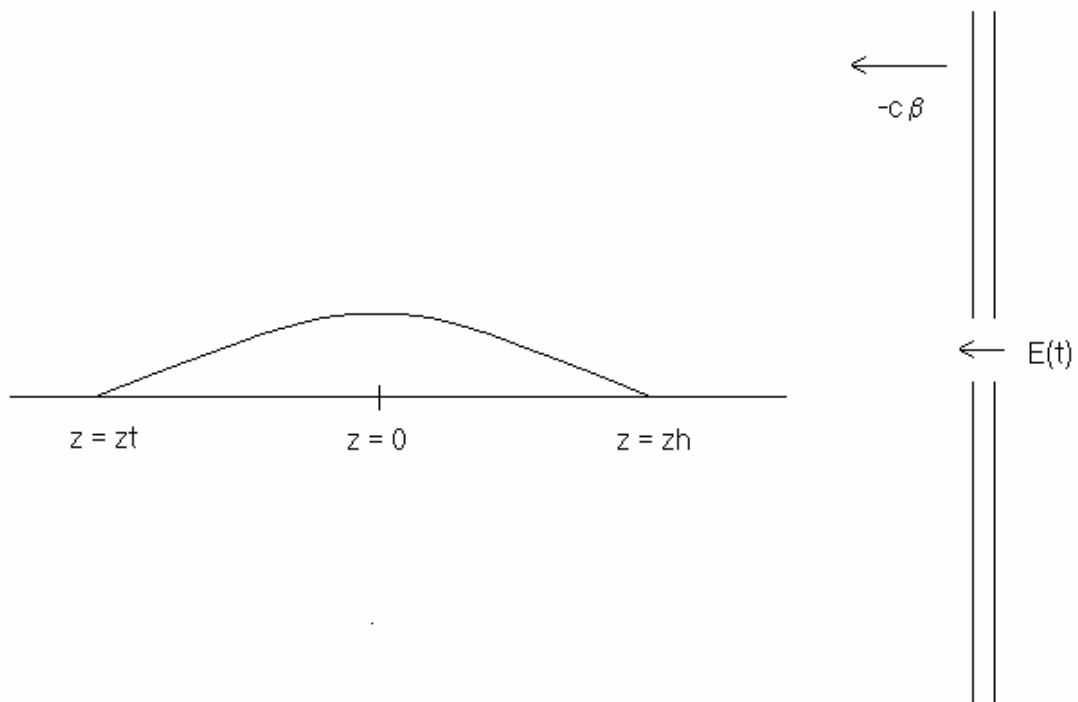


Fig. 11. Conceptual layout of induction gap in the rest frame of the beam. The beam pulse may be any shape, and is not confined to parabolic.

electric field due to space charge, given approximately by eq. (15). Thus, for a momentum distribution of $M_0(z) = mv_0(z)$ before the gap, the momentum distribution after the gap is

$$M(z) = M_0(z) + q \left[E_{sz}(z) - E \left(\frac{z_h - z}{c\beta} \right) \right] \frac{l}{c\beta}. \quad (58)$$

To take advantage of the focusing lattice symmetry, the velocities in the beam frame of every particle must be reversed, therefore:

$$M(z) = -M_0(z) \quad (59)$$

$$-2M_0(z) = q \left[E_{sz}(z) - E \left(\frac{z_h - z}{c\beta} \right) \right] \frac{l}{c\beta} = -2mv_0(z) \quad (60)$$

$$E \left(\frac{z_h - z}{c\beta} \right) = E_{app}(z) = \frac{2mc\beta v_0(z)}{lq} - \frac{g}{4\pi\epsilon_0\gamma^2} \frac{\partial\lambda_0(z)}{\partial z}. \quad (61)$$

$E_{app}(z)$ is the electric field which will reverse the velocity of every particle in the beam, allowing the focusing scheme outlined above to work.

From this equation we can see that the function of E_{app} is twofold -- one part cancels the space charge field, while the other part reverses the particle velocity. However, in order to use this, $v_0(z)$ and $\lambda_0(z)$ must be known for every location in the beam. This data can be determined through analytical means such as the method of characteristics, through simulations, or through careful experimental measurements of the beam properties at the intended location of the first gap.

Since UMER currently produces a beam pulse which is initially rectangular, it is useful to consider the application of eq. (61) to rectangular pulses. If the longitudinal focusing lattice period is extremely short, the beam will still be almost rectangular when

it reaches the first gap. Thus, $\frac{\partial \lambda}{\partial z}$ will be extremely large, while very few particles have been accelerated into the head or tail. Accordingly, the space-charge field term in eq. (61) will dominate, and the electric field needed to properly focus the beam will increase as the longitudinal focusing period decreases. If the longitudinal focusing period is long, the beam will have expanded significantly, so that $\frac{\partial \lambda}{\partial z}$ will be small, and the velocity term in eq. (61) dominates. Because the maximum velocity of the particles in the beam frame is the escape speed, which is independent of the distance traveled by the beam, the maximum focusing voltage will also be independent of the distance traveled by the beam. For UMER, with 100 mA current, 100 ns initial full pulse length, and a gap length of 4 mm, the peak focusing voltage will be 3.61 kV, about ten times larger than for a typical parabolic beam in UMER. Note that the extreme coherent energy spread for a rectangular electron beam pulse with the same parameters is 3.6 keV. This is not coincidence, but rather due to the fact that the induction gap reverses the velocity of every particle in the beam. Thus, the electron at the extreme head of the beam, initially traveling with velocity $2c_0$ in the beam frame, or energy 12.1 keV in the laboratory frame, has its velocity reversed by the gap and is then traveling at $-2c_0$ in the beam frame, or 8.5 keV in the laboratory frame. Because $-2c_0$ is also the initial velocity in the beam frame of the electron at the extreme tail of the beam, the voltage equivalent of the extreme coherent energy spread of the beam, 3.6 kV, will also be the magnitude of the peak focusing voltage applied. For the rectangular pulse, the applied voltage curves are piecewise linear. This is because the velocity distribution is linear, and the line charge

density is quadratic. Since the velocity distribution and $\frac{\partial \lambda}{\partial z}$ are used in eq. (61), the focusing voltage in either edge region will be linear. A different initial distribution may require a nonlinear focusing voltage.

The voltage necessary to focus the rectangular pulse may be higher than is desired for UMER due to safety or other considerations. It is possible to reduce this voltage by altering the initial shape of the beam pulse, which in turn will alter the shape of the beam pulse when it arrives at the first gap. For this purpose, simulations can be performed to determine $v_0(z)$ and $\lambda_0(z)$ at the location of the first gap for a given initial pulse shape, and eq. (61) can be used to find whether the voltage needed to focus the hypothetical beam is below the level desired.

4.3. Drift Compression.

Both focusing schemes discussed in this thesis are different from the drift compression scheme which has been discussed extensively in the literature and was used by D.X. Wang for his experiments in the early 1990's[7]. In the drift compression scheme, the space-charge dominated beam is allowed to expand until the edges have totally eroded and the flat top is totally gone. Instead of a flat top, the line charge density forms a cusp where $\frac{\partial \lambda}{\partial z}$ reverses sign over a very short distance. At this point, the velocity distribution of the particles in the beam is linear in z , and a focusing voltage which is also linear in z is applied to focus the beam. This focusing field is intended to reverse the velocity of every particle in the beam, causing the beam to reverse its expansion. Although this scheme may seem good in principle, it encounters several difficulties in practice. First, the amount of time it takes for the beam to reach the cusp

depends on the line charge density and the pulse length of the beam. Since the induction gap is a physical device which must be placed at a particular location along the beamline, the operators would be strictly limited in their choices of beam current and pulse length once the location for the gap was chosen. Second, the behavior of the beam becomes nonlinear as the cusp is reached, since the forward-going wave and the backward-going wave overlap. It is possible that this may cause unwanted effects such as incorrect focusing and growth in beam entropy and emittance. Finally, drift compression does not properly account for space-charge forces. Ideally, drift compression is a special case of the focusing scheme presented in section 4.2, with induction gaps located exactly where the cusp occurs. This can be taken into account in eq. (61) by taking a velocity $v_0(z)$ which is linear in z . This will naturally occur using the cavitation equation (56d) when the gap is located where the cusp occurs. However, in the drift compression scheme a voltage is applied which is strictly linear in z . This does not properly account for the space charge term in eq. (61), which will not be linear for an expanding, initially rectangular pulse. Although this term is generally negligible, it becomes important near the center of the beam, where $v_0(z) \rightarrow 0$. Because the slope reverses sign at the cusp, the correct applied voltage curve will be broken, with a higher voltage applied at $z = 0^+$ and a lower voltage applied at $z = 0^-$. The magnitude of the difference between these voltages is $\frac{2g}{4\pi\epsilon_0\gamma^2} \frac{\partial\lambda_0}{\partial z} l$. For D.X. Wang's experiment, with beam energy of 0.3 keV, pulse length of 7 ns, current of 3.3 mA, and gap length of 4 mm, this difference is 1.3 V. This difference is small compared to the peak voltage that would need to be applied according to eq. (61), 166 V. However, near the center, the space-charge force correction

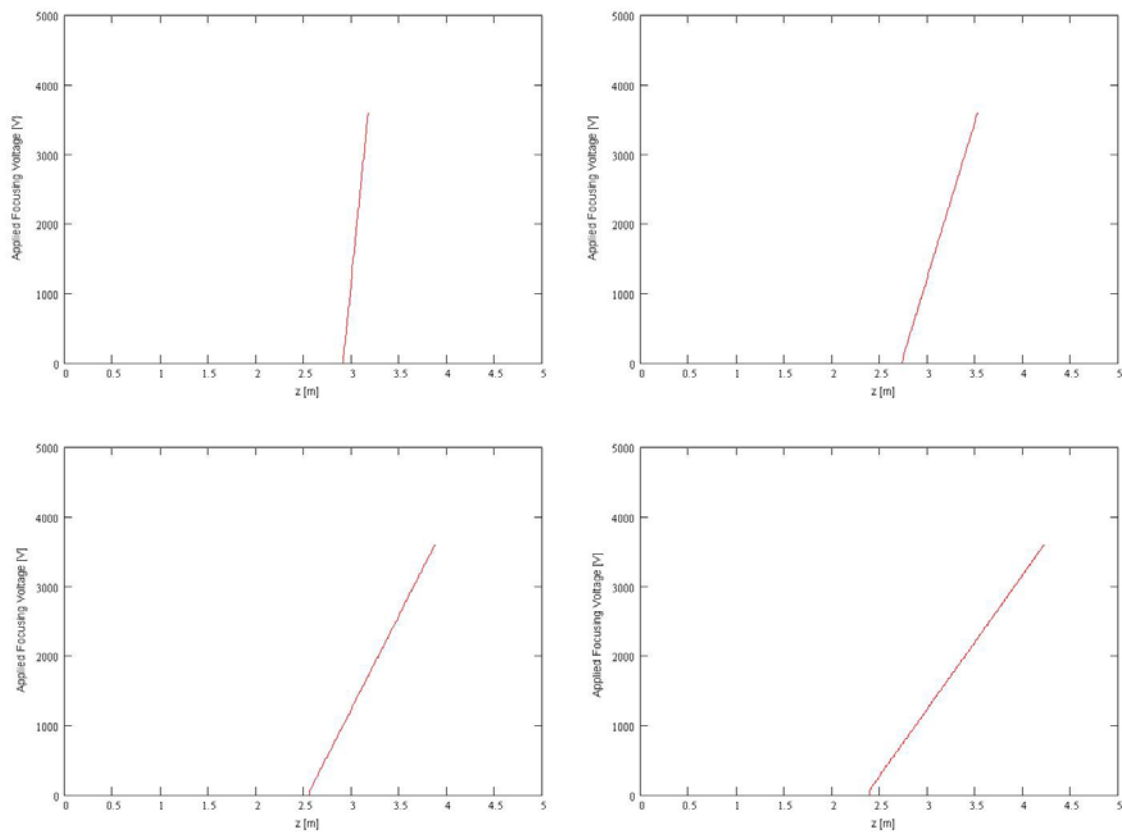


Fig. 12. Voltages needed to properly focus rectangular beam pulse with different focusing period lengths. First induction gap is located at $s = 2$ m, for period of 4 m (top left); first gap at $s = 6$ m, for period of 12 m (top right); first gap at $s = 10$ m, for period of 20 m (bottom left); first gap at $s = 14$ m, for period of 28 m (bottom right). These locations were chosen because they are the actual location of induction gaps in UMER. Curves shown are for head of beam, and corresponding but inverted curves are necessary for focusing the tail of the beam. These curves assume a beam current of 100 mA, initial full pulse length of 100 ns, and a gap length of 4 mm.

is dominant, and it is not clear that it can be neglected. On the other hand, a linear applied voltage *would* be correct if the beam were *parabolic*. In D.X. Wang's experiments, drift compression was used to compress an initially rectangular beam. The resulting compressed beam profile was not rectangular, but rather parabolic. This suggests that the beam may adapt to the external applied potential, adopting a profile which is in equilibrium for that potential. It is also possible that nonlinear effects associated with the cusp caused the beam to adopt an equilibrium distribution. Further research is needed in this area and will be conducted with simulation and the UMER longitudinal focusing system.

5. Additional Effects.

There are several other effects which must be considered in the design of a longitudinal focusing system for UMER. Due to time constraints, these issues have not yet been fully addressed, but will be the subject of future work.

The first such effect is due to the incoherent energy spread of the particles in the beam. Throughout all the work described above, the beam was assumed to be perfectly cold, with emittance being entirely neglected. In fact, although the beams under consideration are space charge dominated, their emittance and incoherent energy spread are not zero. For UMER, the typical incoherent energy spread is about 10 eV. When the particle velocities $v(z)$ are plotted against their locations in the beam z , this incoherent energy spread will have the effect of thickening the curve. Some particles will have velocities greater than the average value of $v(z)$, while some particles will have velocities which are lower. Because only a single value of $v(z)$ is used in eq. (61), the focusing field applied will only correctly focus those particles with velocities of exactly $v(z)$. This means that about half the particles will be slightly underfocused longitudinally, while about half the particles will be slightly overfocused longitudinally. Although it is probably not possible to avoid this effect, it should be possible to determine how prominent it is through simulations.

Two additional effects are related to assumptions made about the nature of the induction gaps. In the process of deriving both eqs. (43) and (61), the electric field in the gaps was assumed to be spatially uniform, as if the induction gap was a parallel plate capacitor. In fact, induction gaps are normally just short gaps in the beam pipe across which a voltage is applied. This means that the electric field in the gap will not be

uniform, but rather that the field strength and direction will be functions of space.

Particles passing along the beam axis will experience more uniform but weaker electric fields than those farther from the beam axis. The first result of this is that there will be a transverse component of the electric field which will cause transverse focusing. If the gap length is small compared to the beam pipe radius, the gap behaves as a transverse focusing element with focal length f given by

$$\frac{1}{f} = \frac{3}{8} \left(\frac{1.318}{b} \right) \left(\frac{V_1}{V_2} \right)^{\frac{1}{4}} \left(\frac{V_1 + V_2}{V_2 - V_1} \ln \frac{V_2}{V_1} - 2 \right) \quad (62)$$

in the nonrelativistic case[12,33]. In this equation, V_1 and V_2 are the voltage equivalents of the momenta of the particles before and after passing through the gap, and the beam pipe radius is $b = 2.54cm$. For a rectangular pulse in UMER, with 100 mA current, $g = 2.8$, and $\beta = 0.2$, the initial kinetic energy of the particle at the extreme head of the beam before focusing is 12.1 keV, and the initial kinetic energy of the particle at the extreme tail of the beam before focusing is 8.5 keV. During the process of longitudinal focusing, these energies are reversed, with the new energy of the particle at the extreme head being 8.5 keV and the new energy of the particle at the extreme tail being 12.1 keV. Thus, for the extreme head $V_1 = 12.1kV$ and $V_2 = 8.5kV$, while for the extreme tail $V_1 = 8.5kV$ and $V_2 = 12.1kV$. Thus the transverse focal length for the particle at the extreme head of the particle is $f = 2.27m$, while the transverse focal length for the particle at the extreme tail of the particle is $f = 2.71m$. The transverse focusing effect decreases from these maximum values at the extreme head and tail, to zero at the inside edge of the head and tail where the velocity (in the beam frame) of the particles drops to zero. The discrepancy between the focal lengths for the head and the tail arises from the

factor of $\left(\frac{V_1}{V_2}\right)^{\frac{1}{4}}$. Note that the focal length of the quadrupole magnets used in UMER is approximately 0.15 m[34]. This means that the transverse focusing effect of the induction gaps in UMER will be weak, but possibly not negligible.

The second result is that the longitudinal component of the electric field will have a radial dependence, causing particles near the center of the beam to experience a different longitudinal focusing force than those particles far from the center. This could cause a telescoping effect where portions of the beam closer to the beam axis are caused to contract faster than those portions far from the beam axis. It is possible that the design of the gap can be altered to reduce these effects.

In addition, the actual geometry and transverse focusing of UMER is different than assumed here. Instead of a linear geometry and uniform transverse focusing, UMER is predominately a circular machine and utilizes transverse quadrupole focusing. Some work by previous researchers indicates that the circular geometry may affect the beam expansion[35]. In addition, quadrupole focusing causes the beam cross section to change area, an effect that was not taken into consideration here. This effect may be similar to a mismatched beam in a uniform focusing channel. Although this also results in envelope oscillations, simulations suggest that effects such as the local change in the geometry factor average out[36].

6. Longitudinal Experiments.

6.1. Introduction.

This thesis has been primarily centered on theoretical aspects of longitudinal focusing in space-charge dominated beams. However, there are a number of effects that can best be investigated directly through experiment. In this section, a series of experiments are proposed that can be carried out before and after the induction gaps are actually installed.

6.2. UMER Facility and Diagnostics.

Because UMER was designed specifically for both transverse and longitudinal experiments, it features an array of diagnostic tools useful for the type of experiments described below. In addition to the standard phosphor screens, which can be used to determine beam radius for calculating g , UMER will include over a dozen Beam Position Monitors (BPMs). Although the primary function of these BPMs is to determine the location of the transverse centroid of the beam to aid in transverse steering, they were developed with the secondary purpose of finding the longitudinal line-charge density profile of the beam as it passes. To this end a compromise was made between their transverse sensitivity and their rise time. Although their rise time is 1-2 ns, through careful design they retain a superior transverse sensitivity[8]. Their fast rise time is particularly important, since the rise time of the beam itself is about 4 ns. Additional line-charge density measurements can be made with fast current monitors, which are available for insertion into the ring. The diagnostics chamber in the extraction system includes a Faraday cup, slit-wire system, and energy analyzer. These tools allow the transverse emittance, beam charge, and longitudinal energy spread to be monitored.

However, because the location and numbers of these detectors are limited, longitudinal measurements, at least in regard to line charge density, will rely on the BPMs.

6.3. Longitudinal Experiments not requiring Induction Gaps.

Fortunately, there are a number of useful longitudinal experiments which do not require induction gaps, and which can be carried out immediately. These experiments all involve free expansion of the beam. Since the UMER beam is approximately a rectangular pulse, with a 4 ns rise time, the behavior outlined in section 3 should apply. Specifically, the expansion of the beam should be linear in time. The whole beam should expand at a rate of $4c_0$, which takes into account the escape speed of the particles at the head and at the tail. The flat top should erode at a rate of $2c_0$. Accordingly, with standard beam parameters for UMER (100 mA current, $\beta = 0.2$, $g = 2.8$, and initial pulse length of 100 ns), the flat top should be totally eroded and the cusp should occur after 1.16 μ s. During this time, the beam center will have traveled downstream for 69.6 m, or 6.1 turns of the ring (neglecting injection section length). This expansion can be monitored using BPMs. Multi-turn operation is desirable but not necessary.

The values quoted above assume that $\alpha = 1$, its generally accepted value. If the observed expansion is linear in time, but occurs at a different rate, this could indicate that the value of g is incorrect. If $\alpha = 0$, and $g = 1.8$, the new speed of sound in the beam will be $c_0 = 2.08 \times 10^6 \frac{m}{s}$, or 80.3% of its value at $g = 2.8$. In this case, the cusp will occur after 1.44 μ s, or when the beam has traveled 86.4 m or about 7.6 turns (neglecting injector section length). These differences are measurable, and will allow us to make an experimental determination of the value of α for UMER.

The transverse quadrupole focusing used in UMER, which causes transverse envelope oscillations, will alter the ratio between the beam pipe radius b and the beam radius a . It is expected, based in part on simulations done previously on transverse mismatch oscillations[36] that the appropriate value of $\frac{b}{a}$ is the average value encountered by the beam as it travels through the system. Because b is essentially uniform in UMER, only the average value of a must be determined from experiment. Even though the ratio of $\frac{b}{a}$ influences g through a logarithm, beam expansion in UMER should be sensitive to changes in the average value of a . If the nominal values of $a = 1cm$ and $b = 2.54cm$ are used, $\ln\left(\frac{b}{a}\right) = 1.86$. However, a 50% increase in a gives $\ln\left(\frac{b}{a}\right) = 1.05$, while a 50% decrease in a gives $\ln\left(\frac{b}{a}\right) = 3.25$. In order to determine α , it will be critical to use an accurate value of the average beam radius. In order to confirm the dependence of the speed of sound in the beam on the beam radius, apertures of varying sizes can be used to alter the initial beam radius.

In addition to varying g , it will be useful to vary the beam current. Changing the beam current, and therefore the line charge density λ_0 , should also allow us to control the speed of sound through eq. (53). UMER's current range of 1 mA - 100 mA should allow a factor of 10 reduction in the speed of sound in the beam. It should also be noted that at $I = 1mA$, UMER is no longer transversely space-charge dominated, although it remains longitudinally space-charge dominated. It is normally assumed that the transverse and longitudinal dynamics are independent of each other. However, this assumption is not

correct in all cases. A comparison of the measured speed of sound in the beam to the speed predicted by the one-dimensional theory will provide a clue to whether this assumption holds for UMER when the longitudinal and transverse intensities are so different. It will also be useful to monitor the transverse and longitudinal temperatures as the beam is allowed to travel over longer and longer distances, and to monitor these values at various beam currents. The large difference between the longitudinal and transverse intensities may enhance the drive towards thermal equilibrium.

Preliminary measurements of the pulse length have been carried out using a 100 mA, 10 keV beam with an initial pulse length of 100 ns. At approximately 3.5 m downstream of the gun, pulse length measurements were taken with two separate systems, the Faraday cup and the slit-wire system. The more accurate slit-wire system gave a pulse length of 110 ns, while the less accurate Faraday cup gave a pulse length of 100 ns. The value of 110 ns is in agreement with the expected expansion of the beam if $g = 2.8$. However, the distance over which the beam traveled before reaching the diagnostics chamber was only an estimate, simply intended to see if the one-dimensional theory gave beam expansion numbers roughly similar to those actually encountered in UMER. Future experiments will be carried out in more detail.

Although it is useful to discuss measurements of the beam flat top and full length, in practice these values are hard to obtain consistently. Instead, most measurements of beam length will be made at 10% and 90% of the peak value. These measurements can easily be compared to the theoretical curves, either directly through eq. (56), or through the software used to produce Fig. 10.

Another goal will be to look for the pulse rounding detected in the data of Faltens[24] and D.X. Wang[7]. If the source of this rounding is due to detector rise time, UMER's improved diagnostics will probably prevent its appearance. It is more likely, due to its appearance in simulations, that this pulse rounding is due to the one-dimensional nature of the cold fluid theory. In either case, better data will be useful in the ongoing efforts to fully explain this discrepancy.

One of the intended purposes of UMER is to further investigate the propagation of space-charge waves, expanding on the efforts of D.X. Wang (longitudinal waves), and S. Bernal (transverse waves)[11]. Ultimately, perturbations will be added to the flat top through the pulser circuit and through combined thermionic and photoelectric emission[37]. Even before these systems are fully operational, it may be possible to get a preview of these effects using the perturbations that naturally occur on the flat top due to impedance mismatches in the pulser circuit. Careful monitoring of the locations of these perturbations as the beam travels downstream should allow us to determine if these perturbations naturally launch longitudinal space-charge waves.

All of the experiments discussed above can be performed before a single induction gap is constructed, and most can be performed immediately, although increased beamline length and multiturn operation are desirable.

6.4. Longitudinal Experiments requiring Induction Gaps.

Once the induction gaps are constructed and placed in the ring, a whole new set of experiments will be possible. As soon as the first gap is placed in the ring, tests can begin on pulse compression. Initially, the goal will be to verify that eq. (61) gives the correct focusing field to provide periodic longitudinal focusing. Although UMER

currently uses a beam pulse which is approximately rectangular it may be desirable to increase the rise time of this pulse so that the applied focusing voltage can be reduced to a more manageable level. It should be noted that by simply reducing the current to 1 mA from 100 mA, the velocity term in eq. (61) can be reduced by a factor of 10. If the decision is made to modify the gun pulse shape, theoretical and simulation efforts will be needed to determine the best compromise shape that: 1) retains a useable flat top, 2) reduces the focusing voltage requirements, and 3) is simple to produce at the gun.

Ideally, the induction gap will allow the initial pulse shape to be recovered. However, since fairly high voltages are applied to the beam over fairly short distances, it is likely that the beam entropy will increase somewhat with every pass through an induction gap. One goal will be to see how well the pulse can be reconstructed, and whether emittance, which is related to entropy, will increase because of the presence of the induction gaps. Monitoring any increase in emittance should be straightforward. First, the beam is allowed to travel a certain number of turns from the gun to the diagnostics chamber, where the transverse emittance is measured. Longitudinal energy spread, which is related to longitudinal emittance by eq. (9), is measured using the energy analyzer. Then, over additional shots, the induction gap voltage is slowly increased to the highest desired level while the waveform shape is retained. Every time the voltage is increased, additional emittance measurements are taken, as well as line-charge pictures using the BPMs. If multiturn operation is available or if multiple induction gaps are installed, further testing can be done.

Multiturn operation or the presence of multiple induction gaps will also be beneficial to looking at irreversibility associated with the cusp. When the cusp occurs,

the forward-traveling and backward-traveling waves overlap, and the system becomes nonlinear. However, it is not clear if this nonlinearity begins to arise before the cusp occurs. In this set of experiments, the beam is allowed to expand for increasingly long periods of time before the induction gaps are used to focus it. The line charge profile will be monitored using the BPMs, and transverse and longitudinal emittance will be monitored using the diagnostics chamber. As the beam is allowed to expand for longer and longer periods of time before focusing, it is expected that longitudinal emittance will increase, and the fully focused beam profile will be less and less like the initial shape, due to increasing entropy. Specifically, we expect the beam to adopt the Boltzmann distribution, which is an equilibrium distribution. This series of tests has particular significance for the design of HIF drivers, since the number of induction gaps may have to be increased in order to reliably and reproducibly refocus those beams.

A third set of longitudinal experiments that can be carried out when the induction gaps are installed involves using the induction gaps to modify the line charge profile in ways other than simply refocusing it. If the beam entropy increase is slow enough, it may be possible that the beam shape will come into equilibrium with whatever induction gap pulse is applied. This conjecture seems to be supported in part by the longitudinal focusing experiments of D.X. Wang, in which a rectangular beam was allowed to expand, and then was refocused as a parabolic shape. A related experiment would be to only apply focusing to the interior of an expanding rectangular beam, and see if some new arbitrary shape could be carved from it.

Throughout all these experiments, it will be important to monitor the longitudinal and transverse temperatures, in order to determine which processes drive the beam towards thermal equilibrium, and how strong those effects are.

7. Conclusion.

The purpose of this thesis has been to explore theoretical aspects of longitudinal focusing in space-charge dominated beams. This began with a brief discussion of beams which are transversely space-charge dominated, as indicated by the intensity parameter χ . The longitudinal envelope equation was introduced, and used to derive a longitudinal intensity parameter χ_L , which is the longitudinal analog to χ . The longitudinal intensity parameter was used to show that UMER will be longitudinally space-charge dominated for all practical operating parameters, although it is able to operate in both the transverse emittance dominated and transverse space-charge dominated regimes. The longitudinal envelope equation was then used to solve for the free-expansion envelope for a space-charge dominated beam, and used to find the focusing field needed for the periodic longitudinal focusing of parabolic beams. The limitations of the parabolic beam profile and the longitudinal envelope equation led to the use of the one-dimensional cold fluid model for modeling rectangular beams. The line charge density and particle velocity distribution derived using the one-dimensional cold fluid model were stated, and used to determine the longitudinal expansion rate, the flat top erosion rate, and the coherent energy spread for a space-charge dominated rectangular beam. To use the line charge and velocity distribution data produced by the one-dimensional cold fluid model, a more general approach to solving for the applied field in a periodic longitudinal focusing system was developed. This method is not limited to use with the rectangular beam, but is applicable for any beam profile for which the line charge density and the velocity distribution are known as functions of position in the beam. The peak voltage needed to focus a 100 mA, 10 keV rectangular beam in UMER was found to be 3.61 kV.

Comparison was made to the conventional drift compression longitudinal focusing scheme, and some problems with that scheme were noted. Several additional effects were noted and a number of longitudinal experiments were proposed.

Future efforts will concentrate on expanding the one-dimensional cold fluid model to non-rectangular line charge distributions; more fully explaining the discrepancies between the one-dimensional cold fluid theory and the three-dimensional simulations and experiments; designing an induction gap system for UMER; and performing longitudinal experiments both with and without the induction gaps.

REFERENCES

- [1] M. Reiser, et al., "The Maryland Electron Ring for Investigating Space-Charge Dominated Beams in a Circular FODO System." *Proc. 1999 Particle Accelerator Conference*.
- [2] T.L. Houck, et al., "Diagnostics for a 1.2 kA, 1 MeV, Electron Induction Injector." *Proc. 1998 Beam Instrumentation Workshop*.
- [3] P. Piot, et al., "A Multislit Transverse-Emittance Diagnostic for Space-Charge-Dominated Electron Beams." *Proc. 1997 Particle Accelerator Conference*.
- [4] M. Reiser and R.A. Kishek, "Transport Studies of Space-Charge Dominated Beams." *NERSC 1998 Annual Report: High Energy and Nuclear Physics*.
- [5] W.M. Sharp, D.A. Callahan, and D.P. Grote, "Longitudinal Dynamics and Stability in Beams for Heavy-Ion Fusion." *Space Charge Dominated Beams and Applications of High Brightness Beams*. Ed. S.Y. Lee. AIP: Woodbury, N.Y. 1996
- [6] P.G. O'Shea, Personal Communication.
- [7] Dunxiong Wang, *Experimental Studies of Longitudinal Dynamics of Space-Charge Dominated Electron Beams*. Doctoral Dissertation, University of Maryland, 1993.
- [8] J. Harris, B. Quinn, et al., "A Fast Beam Position Monitor for UMER." *Proc. 2001 Particle Accelerator Conference*.
- [9] A. Valfells, et al., "Energy Analyzer Experiments for the University of Maryland Electron Ring." *Proc. 2001 Particle Accelerator Conference*.

- [10] P.G. O'Shea, "The University of Maryland Electron Ring." *Proc. 2001 Particle Accelerator Conference*.
- [11] S. Bernal, *Study of Transverse Density Waves in an Electron Beam Experiment*.
Doctoral Dissertation, University of Maryland, 1999.
- [12] Martin Reiser, *Theory and Design of Charged Particle Beams*, Wiley, New York, 1994.
- [13] L. Smith, et al., *ERDA Summer Study of Heavy Ions for Inertial Fusion: Final Report*, LBL-5543, Appendix 6-4, December 1976.
- [14] David Neuffer, "Extensions of the Longitudinal Envelope Equation,"
FERMILAB-TM-1993, April 1997.
- [15] Frank J. Sacherer, *IEEE Trans. Nucl. Sci.* **18**, p. 1105, 1971.
- [16] M. Reiser, Personal Communication, 19 Aug. 2001.
- [17] Y. Cui, "Design Studies for an Experiment to Measure Energy Spread Evolution through a Solenoidal Focusing System." *Proc. 2001 Particle Accelerator Conference*.
- [18] Nathan Brown and Martin Reiser, *Particle Accelerators*, Vol. 43(4), pp. 231-233, 1994.
- [19] Ivan S. Sokolnikoff and Elizabeth S. Sokolnikoff, *Higher Mathematics for Engineers and Physicists*, MacGraw-Hill, New York, 1941, p. 272.
- [20] D.D.-M. Ho, S.T. Brandon, and E.P. Lee, *Particle Accelerators*, Vol. 35, 1991, pp. 15-42.
- [21] Oliver Boine-Frankenheim, "Longitudinal Space Charge Fields," Online:
<http://www-linux.gsi.de/~boine/vorlesung/skript/html/node22.html>, 6 March

2002. This derivation of the space-charge field implicitly assumes that the line charge density is varying slowly.
- [22] I. Haber, et al., "Maryland Transport Experiment Comparison to Theory and Simulation." *Space Charge Dominated Beams and Applications of High Brightness Beams*. Ed. S.Y. Lee. AIP: Woodbury, N.Y. 1996
- [23] I. Haber, Personal Communication.
- [24] A. Faltens, E.P. Lee, and S.S. Rosenblum, *J. Appl. Phys.* **61** (12), 15 June 1987, p. 5219
- [25] D.X. Wang et al., *Appl. Phys. Lett.* **62** (25), 21 June 1993, p. 3232.
- [26] Y. Zou et al., *Phys. Rev. Lett.* **84** (22), 29 May 2000, p. 5138.
- [27] J.D. Jackson, *Classical Electrodynamics*, 3rd. ed., Wiley, New York, 1998.
- [28] H.W. Liepmann and A. Roshko, *Elements of Gasdynamics*, Wiley, New York, 1967.
- [29] G. Emanuel, *Analytical Fluid Dynamics*, CRC, Boca Raton, 2001.
- [30] A.H. Shapiro, *The Dynamics and Thermodynamics of Compressible Fluid Flow*, Vol. II, Ronald, New York, 1954.
- [31] L.D. Landau and E.M. Lifshitz, *Fluid Mechanics*, Pergamon, London, 1959.
- [32] Yupeng Cui, Personal Communication, 20 Aug. 2002.
- [33] Yinbao Chen and M. Reiser, *J. Appl. Phys.* **65** (9), 1 May 1989, p. 3324.
- [34] P.G. O'Shea, Personal Communication, 24 Aug. 2002.
- [35] Rami Kishek, Personal Communication.
- [36] Irving Haber, Personal Communication, 7 Aug. 2002.

- [37] D.W. Feldman, et al., "Combined Thermionic and Photoelectric Emission from Dispenser Cathodes." *Proc. 2001 Particle Accelerator Conference*.